JCI The Journal of Clinical Investigation

RBMS1 regulates lung cancer ferroptosis through translational control of SLC7A11

Wenjing Zhang, … , Han Liu, Yang Wang

J Clin Invest. 2021. https://doi.org/10.1172/JCI152067.

Research In-Press Preview **Cell biology** **Oncology**

Graphical abstract

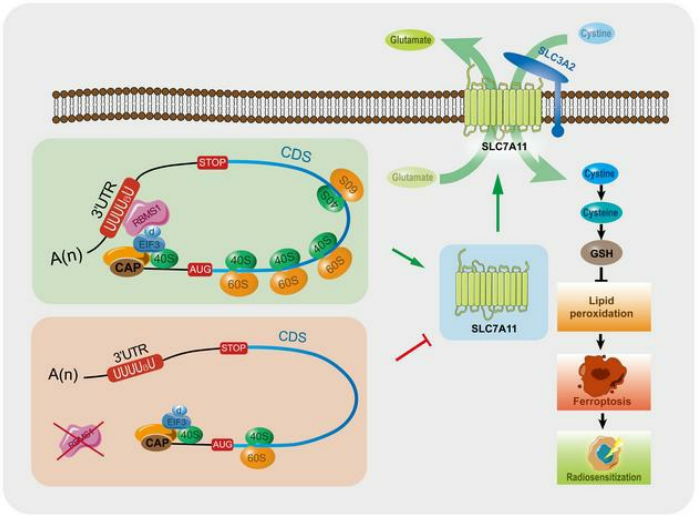

RBMS1 regulates lung cancer ferroptosis through translational control of SLC7A11

Wenjing Zhang[1#], Yu Sun[1#], Lu Bai[1#], Lili Zhi[1#], Yun Yang[2#], Qingzhi Zhao[1], Chaoqun Chen[1], Yangfan Qi[1], Wenting Gao[3], Wenxia He[1], Luning Wang[1], Dan Chen[4], Shujun Fan[5], Huan Chen[6], Hai-long Piao[6], Qinglong Qiao[6], Zhaochao Xu[6], Jinrui Zhang[1], Jinyao Zhao[1], Sirui Zhang[2], Yue Yin[7], Chao Peng[7], Xiaoling Li[8], Quentin Liu[1], Han Liu[1], Yang Wang[1*]

[1]Institute of Cancer Stem Cells and Second Affiliated Hospital, Dalian Medical University, Dalian 116044, China.

[2]CAS-MPG Partner Institute for Computational Biology, Shanghai Institute of Nutrition and Health, Chinese Academy of Sciences, Shanghai 200031, China

[3]Institute of Genome Engineered Animal Models for Human Diseases, Dalian Medical University, Dalian 116044, China

[4]Department of Pathology, First Affiliated Hospital, Dalian Medical University, Dalian 116044, China

[5]Department of Pathology, Dalian Medical University, Dalian 116044, China

[6]CAS Key Laboratory of Separation Science for Analytical Chemistry, Dalian Institute of Chemical Physics, Chinese Academy of Sciences, Dalian 116023, China.

[7]National Facility for Protein Science in Shanghai, Zhangjiang Lab, Shanghai Advanced Research Institute, Chinese Academy of Science, Shanghai 201210, China

[8]Signal Transduction Laboratory, National Institute of Environmental Health Sciences, Research Triangle Park, NC 27709, USA

[#] These authors contributed equally to this work.

[*] Correspondence:

Yang Wang; Institute of Cancer Stem Cells and Second Affiliated Hospital, Dalian Medical University, Dalian, China 116044; Tel: +86-411-86110531; Email: yangwang@dmu.edu.cn

The authors have declared that no conflict of interest exists.

Running title: Depleted RBMS1 inhibits tumorigenesis via promoting ferroptosis

Abstract

Ferroptosis, an iron-dependent non-apoptotic cell death, is a highly regulated tumor suppressing process. However, functions and mechanisms of RNA binding proteins in regulation of evasion of ferroptosis during lung cancer progression are still largely unknown. Here we reported that the RNA binding protein RBMS1 participated in lung cancer development through mediating ferroptosis evasion. Through an shRNA-mediated systematic screen, we discovered that RBMS1 was a key ferroptosis regulator. Clinically, RBMS1 was elevated in lung cancer and its high expression was associated with reduced patient survival. Conversely, depletion of RBMS1 inhibited lung cancer progression both in vivo and in vitro. Mechanistically, RBMS1 interacted with the translation initiation factor eIF3d directly to bridge the 3′- and 5′-UTRs of *SLC7A11*. RBMS1 ablation inhibited the translation of SLC7A11, reduced SLC7A11-mediated cystine uptake and promotes ferroptosis. In a drug screen that targeted RBMS1, we further uncovered that nortriptyline hydrochloride decreased the level of RBMS1, thereby promoting ferroptosis. Importantly, RBMS1 depletion or inhibition by nortriptyline hydrochloride sensitized radioresistant lung cancer cells to radiotherapy. Our findings established RBMS1 as a translational regulator of ferroptosis and a prognostic factor with therapeutic potentials and clinical values.

Keywords: RBMS1, lung cancer, ferroptosis, SLC7A11, translation, eIF3d

Introduction

Ferroptosis, an iron-dependent form of non-apoptotic cell death, is induced by cystine depletion and massive lipid peroxidation-controlled membrane damage (1-4). Dysregulation of ferroptosis has been closely associated with human cancers (5, 6). Accumulating evidence has demonstrated that ferroptosis plays a vital role in tumor suppression (7-9). Traditional chemotherapeutic drugs (e.g. cisplatin) combined with ferroptosis inducers can synergistically inhibit tumor proliferation in head and neck cancer (10). Activation of ferroptosis is able to prevent acquired resistance of cancer cells to several cancer therapies, including lapatinib, erlotinib, and vemurafenib (11-13). Moreover, immunotherapy with anti-PD-L1 antibodies stimulates lipid peroxidation-dependent ferroptosis in tumor cells, ferroptosis and immunotherapy can therefore synergistically inhibit tumor growth in vitro and in vivo (14). Importantly, ferroptosis can also be induced by irradiation and is as important as apoptosis in irradiation-induced tumor suppression (15, 16), implying that activation of ferroptosis might sensitize radioresistant cancer cells to radiotherapy. Therefore, targeting ferroptosis provides great potentials for cancer therapy.

Ferroptosis can be regulated by multiple critical factors, including solute carrier family 7 member 11 (SLC7A11, the key transporter of cystine), and glutathione peroxidase 4 (GPX4) (17-20). SLC7A11 imports extracellular cystine into the cell (21), which is subsequently converted to glutathione (GSH). GPX4 is capable of using GSH to decrease lipid hydroperoxides, thereby inhibiting ferroptosis (17). Thus, SLC7A11 and GPX4 are suppressors of ferroptosis, and inhibition of SLC7A11 or GPX4 with distinct approaches is able to trigger ferroptosis (1)(17). The expression and activity of SLC7A11

is regulated by multiple layers. Under oxidative stress, the transcription factor nuclear factor erythroid 2-related factor 2 (NRF2) binds to the antioxidant response elements (AREs) in the promotor region of *SLC7A11* to stimulate its transcription (22). The transcription of *SCL7A11* can also be regulated by the methylation of histone H3 and BAP1 (7, 23). Apart from transcriptional regulation, the level of *SLC7A11* is also controlled by posttranslational regulation. For instance, OTUB1, a non-canonical deubiquitinase, interacts with SLC7A11 to prevent it from degradation (24). The adhesion molecule CD44 variant (CD44v) serves as a binding partner of SLC7A11 to modulate its protein stability (25). However, despite these observations, translational regulators of ferroptosis during lung cancer progression, are still largely unknown.

RNA-binding proteins (RBPs) are a diverse group of proteins that interact with RNAs to form ribonucleoprotein complex, regulating the fate of their target RNAs and controlling various aspects of gene expression, such as RNA stability, pre-mRNA splicing, translation, and so on (26, 27, 28). Importantly, RBPs are involved in the regulation of a variety of cancer related biological processes, including apoptosis, EMT, as well as autophagy (29-31). However, the role of RBPs in regulating ferroptosis in lung cancer is still elusive. The RNA binding protein RBMS1 (also known as MSSP-1) has been originally identified as the c-Myc gene single-strand binding protein, which could suppress transcription of target genes (32). Recently, RBMS1 was found to directly bind its target mRNAs to modulate RNA stability, thereby inhibiting colon cancer metastasis (33). However, the involvement of RBMS1 in lung cancer through translational regulation of ferroptosis-related genes has not yet been reported. Here we systematically identified RBMS1 as a translational promoting factor of SLC7A11 in lung cancer, and

revealed that depletion of this RNA-binding protein stimulates ferroptosis, thus to inhibit lung cancer cell growth and sensitize lung cancer cells to radiotherapy.

Results

Systematic identification of RBMS1 as a key regulator of ferroptosis in lung cancer

To systematically identify RNA binding proteins that could regulate ferroptosis in lung cancer cells, we carried out an RNAi screen with an shRNA library targeting about two hundred RBPs. The efficacy of this library has been previously validated by the ENCODE project (34). We induced ferroptosis using erastin in the RBPs-depleted lung cancer cells, then measured cell viability in response to ferroptosis induction (Figure 1A). We found that multiple RBPs could participate in regulation of ferroptosis, and subsequently chose the top ten candidate RBPs for further validation (Figure 1B). The RNA binding protein RBMS1 was identified as the top hit that substantially influenced ferroptosis (Figure 1B). As shown in Figure 1C, A549 lung cancer cells with depletion of RBMS1 were extremely sensitive to erastin-induced ferroptosis, and this sensitivity was prevented by the ferroptosis inhibitor Ferrostatin-1 (Ferr-1) (Figure 1C and Supplemental Figure 1A), suggesting that depletion of RBMS1 promotes ferroptosis in lung cancer cells.

To further investigate the potential role of RBMS1 in ferroptosis, we generated RBMS1 stably depleted H1299 lung cancer cells with two independent shRNAs and found that knockdown of RBMS1 notably elevated erastin-triggered lipid peroxidation (Figure 1D and Supplemental Figure 1B). Consistently, CRISPR-mediated deletion of RBMS1 also increased erastin-induced lipid peroxidation in H1299 lung cancer cells (Supplemental Figure 1C). Transmission Electron microscopy (TEM) analysis further revealed that RBMS1 depleted lung cancer cells contained shrunken mitochondria with elevated membrane density, a typical morphologic feature of ferroptosis (Figure 1E).

Similar results were also observed in RBMS1-depleted H1299 cells stained with a known mitochondria-tracker-probe Rho123 using Structured Illumination Microscopy (SIM) approach (Figure 1F).

Functionally, reduction of RBMS1 significantly promoted erastin-induced cell death (Figure 2A), which could be prevented by Ferr-1, in different lung cancer cells (Figure 2B and Supplemental Figure 1D). As controls, inhibitors of other forms of cell death, including apoptosis (Z-VAD-fmk) and autophagy (3-methylademine, 3-MA) failed to suppress the erastin-triggered increase of cell death in distinct RBMS1 stably depleted lung cancer cells (H1299 and A549 cells) (Figure 2C-2D and Supplemental Figure 1E), indicating that the erastin-triggered cell death was independent of apoptosis and autophagy in lung cancer cells with stable depletion of RBMS1. Knocking out of RBMS1 in lung cancer cells led to similar results (Supplemental Figure 2A-2E).

To further confirm that RBMS1 deficiency sensitizes lung cancer cells to ferroptosis, we induced ferroptosis with tert-butyl hydroperoxide (TBH), an ROS inducer, in control and RBMS1 knockout lung cancer cells. Deletion of RBMS1 in H1299 cells significantly increased cell death, which could be also substantially suppressed by the ferroptosis inhibitor Ferr-1 but not by the apoptosis inhibitor Z-VAD-fmk or the autophagy inhibitor 3-MA (Figure 2E and Supplemental Figure 3A-3B). Furthermore, knockdown of RBMS1 also sensitized H1299 cells to low-cystine medium-induced ferroptosis, and this sensitivity was fully rescued by Ferr-1 (Figure 2F-2G). Subsequent re-expression of RBMS1 back into H1299 cells with stable RBMS1 depletion markedly reversed the erastin-induced ferroptosis and significantly reduced cell death (Figure 2H-

2I and Supplemental Figure 3C). Altogether, our results demonstrated that loss of RBMS1 stimulates ferroptosis in lung cancer cells.

RBMS1 is associated with lung cancer progression and prognosis in humans and mice

Our identification of RBMS1 as a key regulator of ferroptosis in lung cancer cells raises the possibility that RBMS1 may participate in lung cancer progression by regulating ferroptosis evasion. To test this possibility, we sought to directly evaluate its clinical importance in lung cancer patients. We examined the expression of RBMS1 by immunohistochemistry (IHC) staining using serial sections of tissue microarrays (TMAs) containing lung cancer tissues (n = 60), and the matched adjacent lung tissues (n = 60) (Figure 3A). Specifically, more than 50% of lung cancer samples exhibited strong or extra-strong staining for RBMS1, whereas only less than 5% of adjacent lung tissues displayed strong or extra-strong staining for RBMS1 (Figure 3B). Moreover, lung cancer patients with a higher expression level of RBMS1 usually had a higher clinical stage tumor (Supplemental Figure 4A), indicating that the expression level of RBMS1 was positively correlated to the clinical stages of lung cancer patients. Furthermore, lung cancer patients with relative high levels of RBMS1 had shorter overall survival than those with low levels of RBMS1 (Figure 3C). Therefore, our clinical observations indicate that RBMS1 is a potential prognostic factor in lung cancer.

We next investigated the impacts of RBMS1 on lung cancer progression in mice using a conditional RBMS1 knockout (CKO) strain in which the homozygous floxed *Rbms1* allele (*Rbms1*$^{fl/fl}$) was crossed into the *LSL-Kras*$^{G12D/WT}$ background

(*Kras*$^{G12D/WT}$/*Rbms1*$^{fl/fl}$), with *Kras*$^{G12D/WT}$/*Rbms1*^{WT} as controls (Supplemental Figure 4B-4C). Adeno-associated virus expressing Cre-recombinase-GFP (AAV-Cre-GFP) were introduced into *Kras*$^{G12D/WT}$/*Rbms1*^{WT} *and Kras*$^{G12D/WT}$/*Rbms1*$^{fl/fl}$ CKO mice to induce the knockout of RBMS1 and expression of Kras^{G12D} protein. The equal introduction of GFP-Cre signals were monitored to exhibit in the lung (Supplemental Figure 4D). Strikingly, when imaged at 3-, 5-, and 8- weeks post AAV-Cre infection with coronal and transverse section Micro-Computed Tomography (Micro-CT) scan, both female and male *Kras*$^{G12D/WT}$/*Rbms1*$^{fl/fl}$ CKO mice had much less detectable nodules than *Kras*$^{G12D/WT}$/*Rbms1*^{WT} mice in the lung (Figure 3D and Supplemental Figure 4E-4F). Further tumor analysis revealed that *Kras*$^{G12D/WT}$/*Rbms1*$^{fl/fl}$ CKO mice showed a noticeably reduced tumor area and tumor burden as compared to *Kras*$^{G12D/WT}$/*Rbms1*^{WT} mice (Figure 3E and Supplemental Figure 4G). As expected, compared with tumor tissues from *Kras*$^{G12D/WT}$/*Rbms1*^{WT} mice, tumor sections from *Kras*$^{G12D/WT}$/*Rbms1*$^{fl/fl}$ CKO mice exhibited dramatically decreased levels of RBMS1 but increased levels of 4-hydroxy-2-noneal (4HNE, a biomarker of lipid peroxidation), as judged by IHC staining (Figure 3F). Therefore, consistent with our observations from clinical samples, our findings in mice support the notion that loss of RBMS1 significantly inhibits lung cancer progression, and this inhibition is associated with increased ferroptosis marker (4HNE) staining.

Loss of RBMS1 inhibits lung cancer progression in cultured cells

We further examined the RBMS1 level in a panel of lung cancer cell lines, and found that RBMS1 is markedly increased in multiple lung cancer cell lines as compared to normal bronchial cell lines (Figure 4A). Depletion of RBMS1 significantly inhibited

cell growth of H1299 and A549 lung cancer cells (Figure 4B and Supplemental Figure 5A). In addition, RBMS1 knockdown significantly inhibited anchorage-dependent growth in both H1299 and A549 lung cancer cells as judged by a colony formation assay (Figure 4C and Supplemental Figure 5B). This RBMS1 knockdown-induced growth inhibition was associated with significantly suppressed cell proliferation in H1299 and A549 lung cancer cells, as judged by EdU staining (Figure 4D and Supplemental Figure 5C). Similar growth inhibition was also observed in RBMS1 deleted H1299 and A549 lung cancer cells (Supplemental Figure 5D-5G). Again, RBMS1 deletion-resulted growth suppression could be partially rescued by ferroptosis inhibitors Ferr-1 and liproxstatin-1 (Lip) but not other cell death inhibitors, indicating the depletion of RBMS1 inhibits cell growth in a ferroptosis-dependent manner (Supplemental Figure 5H). To further test whether RBMS1 reduction inhibits lung cancer cells growth in vivo, we subcutaneously injected H1299 lung cancer cells carrying a doxycycline-inducible shRNA of RBMS1 into flanks of nude mice, then fed them with or without water containing doxycycline to deplete RBMS1 (Figure 4E). The growth of tumors was measured every three days, and xenograft tumors were removed for final analysis. Consistent with our observation in vitro, H1299 cells with depletion of RBMS1 grew much slower than controls and developed smaller tumors compared to control cells (Figure 5F-5H). Therefore, loss of RBMS1 inhibits lung cancer progression both in cultured cells and in xenograft tumors.

Depletion of RBMS1 inhibits lung cancer progression partially through the reduction of SLC7A11 and subsequent activation of ferroptosis

To better understand the molecular mechanisms underlying RBMS1-regulated ferroptosis in lung cancer, we performed quantitative proteomics assay using lung cancer cells with doxycycline-induced depletion or overexpression of RBMS1. Intriguingly, the protein level of SLC7A11, a key suppressor of ferroptosis, was significantly decreased upon RBMS1 depletion (Figure 5A and Supplemental Figure 6A, Supplementary Table 1). We confirmed that the expression of SLC7A11 was markedly reduced in the RBMS1-depleted H1299 and A549 lung cancer cells by either stable or transient knockdown, however, the levels of other ferroptosis regulators, including ACSL4, AIFM2, GPX4, and DHODH (35), were not affected (Figure 5B and Supplemental Figure 6B-6C). Conversely, stable overexpression of RBMS1 elevated the expression level of SLC7A11 but not other ferroptosis regulators, in both H1299 and A549 cells (Figure 5B and Supplemental Figure 6C). In addition, re-expression of RBMS1 in lung cancer cells with RBMS1 stable depletion rescued the RBMS1 reduction-induced decrease of SLC7A11 (Supplemental Figure 6D). Since SLC7A11 regulates the uptake of extracellular cystine, a major precursor for glutathione biosynthesis, we subsequently examined the cystine uptake and found that knockdown of RBMS1 significantly decreased the uptake of extracellular cystine (Figure 5C) and significantly decreased the levels of GSH (Figure 5D). Similar results were also obtained in H1299 lung cancer cells with doxycycline-induced depletion of RBMS1 (Supplemental Figure 6E). In addition, depleted RBMS1 notably elevated lipid peroxidation (Figure 5E). Importantly, restoration of SLC7A11 in RBMS1-knockdown or RBMS1-deleted H1299 lung cancer cells almost fully suppressed erastin-triggered cell death (Figure 5F-5H, Supplemental Figure 6F-6I).

Notably, re-expression of SLC7A11 in RBMS1-depleted H1299 lung cancer cells inhibited lipid peroxidation triggered by low-cystine medium (Figure 6A and Supplemental Figure 7A) and reversed the low-cystine medium-induced cell death (Figure 6B and 6C). Moreover, addition of N-acetylcysteine (NAC) to RBMS1-depleted cells with cystine-deficiency could rescue the RBMS1 depletion-induced cancer cell growth inhibition, suggesting that such effect is dependent on cystine uptake via SLC7A11 (Supplemental Figure 7B). Taken together, our data indicate that RBMS1 depletion promotes ferroptosis mainly through repressing SLC7A11 expression and further suggest that decreased RBMS1 might inhibit lung cancer progression at least partly through suppression of SLC7A11 and promotion of ferroptosis.

To test this hypothesis, we stably transfected RBMS1 depleted H1299 and A549 lung cancer cells with a construct expressing SLC7A11 or the control vector (Supplemental Figure 7C). Restoration of SLC7A11 in RBMS1 stably depleted lung cancer cells partially restored RBMS1 knockdown-induced suppression of cell growth (Figure 6D and Supplemental Figure 7D). In addition, the proliferative ability of RBMS1 depleted lung cancer cells was significantly promoted by SLC7A11 re-expression as judged by colony formation assay and EdU staining (Figure 6E-6F and Supplemental Figure 7E-7F). Consistently, RBMS1 depletion-induced inhibition of xenograft tumor development was also significantly rescued with restoration of SLC7A11 or the treatment with the ferroptosis inhibitor liproxstatin-1, suggesting that such tumor suppression is also dependent on ferroptosis in xenograft mice model (Figure 6G-6I and Supplemental Figure 7G and 7H). Further examination of lipid peroxidation by IHC staining of 4-hydroxy-2-noneal (4HNE) revealed that RBMS1-depleted tumors had increased 4HNE

staining compared to control tumors, but this increase was markedly reduced upon re-expression of SLC7A11 (Figure 6J). Together, our results indicate that loss of RBMS1 suppresses lung cancer progression partially through repressing SLC7A11 and promoting ferroptosis both in vitro and in vivo.

RBMS1 regulates the translation of SLC7A11

We next aimed to understand how depletion of RBMS1 suppresses the expression of SLC7A11. Previously, RBMS1 has been shown to function as a post-transcriptional regulator of RNA stability to modulate gene expression (33). We thus sought to investigate whether RBMS1 affects the mRNA expression of SLC7A11. Surprisingly, the mRNA level of *SLC7A11* was not affected by RBMS1 as judged by qRT-PCR in both the RBMS1 stably depleted lung cancer cells and RBMS1 transiently knocked down lung cancer cells with siRNAs (Figure 7A and Supplemental Figure 8A). This observation suggests that RBMS1 might regulate the expression of *SLC7A11* at the post-RNA level, including translation.

To directly examine whether RBMS1 regulates the translation of SLC7A11, we generated four translation reporters using different promoter and UTR fragments from *SLC7A11* (SLC7A11-fluc-FL, SLC7A11-fluc-T1, SLC7A11-fluc-T2, and SLC7A11-fluc-T3) (Figure 7B). We conducted luciferase reporter assay and found that the activity of luciferase reporter SLC7A11-fluc-FL was significantly inhibited by depleted RBMS1 in lung cancer cells, however, the mRNA level of SLC7A11-fluc-FL was not affected (Figure 7C). Moreover, only the activity of luciferase reporter SLC7A11-fluc-T3, but not SLC7A11-fluc-T1 and SLC7A11-fluc-T2, was significantly suppressed in RBMS1

depleted lung cancer cells (Figure 7D and Supplemental Figure 8B), suggesting that RBMS1 regulates the translation of SLC7A11 protein through the second half of its 3′-UTR (the T3 region). In support of this idea, multiple RBMS1 binding sites (e.g. AU-rich sequence) were found in the T3 region, and truncated mutations of partial binding sites (SLC7A11-fluc-T4 or SLC7A11-fluc-T5) could not totally abolish such repressive function (Supplemental Figure 8C). Additionally, re-expressing RBMS1 overturned the RBMS1 depletion-induced luciferase activity suppression of the reporter SLC7A11-fluc-T3 (Figure 7E and Supplemental Figure 8D). We further analyzed actively translated mRNAs by Ribo-Seq analysis and identified a number of active translated mRNAs whose translation might be controlled by RBMS1, with SLC7A11 as one of the top targets (Figure 8). Consistent with this observation, immunofluorescence assay showed that RBMS1 was co-localized with Calnexin, an ER marker, suggesting that RBMS1 might localize at ER to regulate translation (Supplemental Figure 8E). Together, our results indicate that RBMS1 is capable of promoting the translation of *SLC7A11* through the downstream region of its 3′-UTR.

RBMS1 interacts with eIF3d to bridge the 3′- and 5′-UTR of SLC7A11 to promote its translation

To better understand how RBMS1 regulates the translation of SLC7A11, we pulled down RBMS1-containing immunocomplex from cells stably expressing RBMS1 and determined its associated proteins using Mass-Spectrometry assay. Cells containing empty vector were used as controls. Totally, one hundred and eighteen proteins have been specifically identified. When analyzing cellular functions of potential RBMS1-

interacting proteins using gene ontology, we found that the interacting proteins were mostly enriched in multiple translation-related pathways, including translation regulation, translation initiation, and ribonucleoprotein biogenesis (Figure 9A). Further STRING analysis revealed that RBMS1-interacting proteins were functionally clustered into a few well-linked interaction networks, including the expected RNA processing subgroup (Figure 9B). However, remarkably, proteins involved in the regulation of translation formed the other major subgroup (Figure 9B). Therefore, our results further prove that RBMS1 might regulate the expression of *SLC7A11* through control of translation.

Strikingly, multiple key translation regulators, including cap-binding protein eukaryotic initiation factor 3d (eIF3d), eIF3i, and eIF3m, were identified in the immunoprecipitation (IP) coupled Mass-Spectrometry assay using exogenously expressed RBMS1 as a bait. These factors are critical components of eIF3 complex that could drive a cap-dependent pathway of translation initiation (36). We confirmed that exogenously expressed eIF3d, eIF3i, and eIF3m could pull down the endogenous RBMS1 respectively in a co-IP assay (Figure 9C). Conversely, exogenously expressed RBMS1 pulled down endogenous eIF3d, eIF3i, and eIF3m in both H1299 and A549 cells respectively as well (Figure 9D and Supplemental Figure 9A). The expression levels of eIF3d, eIF3i, and eIF3m were not affected by RBMS1 (Supplemental Figure 9B). Interestingly, the interaction between RBMS1 and eIF3m was dependent on RNA as the RNase treatment abolished their interaction in a Co-IP assay (Figure 9E). Furthermore, an in vitro pull-down assay using purified proteins showed that GST-RBMS1 pulled down His-eIF3d, but not His-eIF3i nor His-eIF3m, indicating that RBMS1 is able to directly interact with eIF3d (Figure 9F and Supplemental Figure 9C). Importantly, Proximity

Ligation Assay (PLA), a powerful tool that allows in situ detection of endogenous protein interactions with high specificity and sensitivity, confirmed that RBMS1 indeed interacted with endogenous eIF3d in the cytoplasm (Figure 9G and Supplemental Figure 9D). Taken together, our data suggest that RBMS1 might regulate the translation of *SLC7A11* through directly interacting with eIF3d.

To test this possibility, we overexpressed eIF3d together with the luciferase reporters of *SLC7A11*. As expected, overexpression of eIF3d significantly promoted the activity of luciferase reporter SLC7A11-fluc-T3, but not SLC7A11-fluc-T2, in lung cancer cells (Figure 10A and Supplemental Figure 9E). Interestingly, eIF3d-induced activation of SLC7A11-fluc-T3 reporter was abolished in RBMS1-depleted cells (Figure 10B and Supplemental Figure 9F), indicating the translational activation of *SLC7A11* by eIF3d is dependent on RBMS1. Conversely, depletion of eIF3d noticeably reduced the protein level of *SLC7A11*, and suppressed the RBMS1-induced increase of SLC7A11 (Figure 10C-10D). Collectively, our results demonstrate that eIF3d plays a vital role in RBMS1-regulated *SLC7A11* translation.

We next sought to study how RBMS1 coordinates with eIF3d to regulate the translation of *SLC7A11*. Generally, translational regulators bind to the 5′- or 3′-UTR of target genes to modulate the translation. We therefore performed an RNA-IP assay with RBMS1 or eIF3d stably overexpressed A549 and 293T cells. RBMS1 and eIF3d bound to both the 5′- and 3′-UTR of *SLC7A11* in the RNA-IP assay (Figure 10E-10F, and Supplemental Figure 9G). However, depletion of RBMS1 largely abolished the binding of eIF3d to the 3′-UTR, but not the 5′-UTR of *SLC7A11*, suggesting that eIF3d binds to 3′-UTR of *SLC7A11* through interacting with RBMS1 (Figure 10G and Supplemental

Figure 9H). Additionally, knockdown of eIF3d almost disrupted the binding of RBMS1 to the 5′-UTR, but not the 3′-UTR of *SLC7A11*, indicating that RBMS1 binds to the 5′-UTR of *SLC7A11* via interacting with eIF3d (Figure 10H and Supplemental Figure 9I). Thus, these data suggest that eIF3d is associated with the 3′-UTR of *SLC7A11* through RBMS1, whereas RBMS1 binds to the 5′-UTR of *SLC7A11* through eIF3d. Taken together, our results support a model in which RBMS1 binds to eIF3d complex to bridge the 3′- and 5′-UTR of *SLC7A11*, which in turn promotes the translation of *SLC7A11* (Figure 10I).

RBMS1 positively correlates to elevated SLC7A11 in clinical samples and confers lung cancer cell resistance to radiotherapy

Since RBMS1 depletion-induced translational repression of SLC7A11 promotes ferroptosis and inhibits lung cancer progression, we examined the expression of RBMS1 and SLC7A11 in surgically collected paired NSCLC samples and adjacent normal tissues from seven patients. Remarkably, all NSCLC specimens had markedly increased RBMS1 and SLC7A11 protein levels as compared to matched adjacent normal tissues (Figure 11A), and the level of SLC7A11 is positively correlated to that of RBMS1 in clinical samples ($R^2 = 0.893$, $P < 0.0001$) (Figure 11B). Such observation was validated by IHC staining using the same tissue microarrays used in Figure 3A (Figure 11C and Supplemental Figure 10A). Importantly, more than 50% of lung cancer samples showed strong or extra-strong staining for SLC7A11, however, only less than 5% of adjacent lung tissues displayed strong staining for SLC7A11 (Figure 11D). In addition, lung cancer patients with a higher expression level of SLC7A11 likely had a higher clinical

stage tumor (Supplemental Figure 10B), suggesting that the expression level of SLC7A11 is positively correlated to the clinical stages of lung cancer patients. Moreover, lung cancer patients with a relative high level of SLC7A11 had shorter overall survival than those with a low level of SLC7A11 (Figure 11E). Therefore, our clinical observations reveal that RBMS1 is positively correlated to SLC7A11 in lung cancer patient samples, further proving that the clinical value of RBMS1 in lung cancer is through regulating ferroptosis.

In addition, tumor sections from *Kras*$^{G12D/WT}$/*Rbms1*$^{fl/fl}$ CKO mice showed noticeably reduced levels of SLC7A11 than those in tumor tissues from *Kras*$^{G12D/WT}$/*Rbms1*^{WT} mice, as judged by the IHC staining (Figure 11F), further confirming that RBMS1 deficiency-inhibited lung cancer development is associated with reduced expression of SLC7A11 in mice. We also obtained mouse embryonic fibroblasts (MEFs) from *Rbms1*$^{fl/fl}$ mice and found that MEFs with deletion of RBMS1 had a notable decrease of SLC7A11 as judged by a western blot assay (Figure 11G). Functionally, deletion of RBMS1 significantly promoted erastin-induced cell death, which could be prevented by Ferr-1, in MEF cells (Figure 11H). Therefore, our data supported the notion that RBMS1 facilitates lung cancer progression partially through SLC7A11-induced evasion from ferroptosis in mice.

Radiotherapy is one of the most effective routes for lung cancer therapy. It has been previously shown that ionizing radiation (IR) induces ferroptosis, and that SLC7A11 is able to promote radioresistance mainly through suppressing ferroptosis (15). Our observation that SLC7A11 is under translational control of RBMS1 in lung cancer cells and mice raises the possibility that depletion of RBMS1 could partly sensitize IR-

resistant lung cancer cells to radiotherapy through suppressing SLC7A11 expression and promoting ferroptosis. To test this possibility, we employed IR-resistant and parental A549 lung cancer cells (Supplemental Figure 10C) (37) and found that the expression level of RBMS1 was increased in IR-resistant A549 cells regardless of irradiation (Figure 12A). The level of SLC7A11 was also elevated in the IR-resistant cells as compared to the parental cells (Figure 12A). Interestingly, knockdown of RBMS1 in IR-resistant A549 cells decreased the level of SLC7A11 (Figure 12B), induced more lipid peroxidation (Figure 12C), and significantly sensitized these cells to irradiation (Figure 12D). Again, Ferr-1 treatment reversed loss of RBMS1-induced radiation sensitization in IR-resistant A549 cells (Figure 12E). Similarly, knockdown of RBMS1 had synergistic effects with irradiation on radiosensitivity of H1299 cancer cells, which were abrogated by re-expression of SLC7A11 (Supplemental Figure 10D-10E). Collectively, our data demonstrate that RBMS1 positively correlates to elevated SLC7A11 in clinical samples and confers lung cancer cells resistance to radiotherapy. Our findings further suggest that the RBMS1-SLC7A11 axis could be a potential novel therapeutic target for sensitization of lung cancer to radiotherapy.

Nortriptyline hydrochloride inhibits RBMS1 expression and sensitizes IR-resistant lung cancer cells to irradiation through promoting ferroptosis

To further evaluate the therapeutic potential of the RBMS1-SLC7A11 axis for lung cancer treatment, we performed a chemical screen to systematically identify inhibitors of RBMS1 that might promote ferroptosis using the US drug collection of compounds, which contains 1280 drugs (38). We generated H1299 lung cancer cells with

stable expression of EGFP-RBMS1 fusion protein, then incubated these cells with distinct compounds for 12 hours (2μM) (Figure 12F). Totally, eight compounds were identified to reduce fluorescence of EGFP-RBMS1 (Figure 12G). Nortriptyline hydrochloride (NTP), an antidepressant reagent that inhibits the vascular Kv channel (39), was one of the top hits that suppressed the expression of RBMS1 (Figure 7O). We validated that NTP decreased the level of RBMS1 and significantly inhibited the activity of luciferase reporter SLC7A11-fluc-T3 in lung cancer cells (Figure 12H).

Importantly, NTP suppressed the expression of RBMS1 in IR-resistant A549 lung cancer cells and reduced the level of SLC7A11 (Figure 12I) without affecting the expression of other ferroptosis-related factors (Supplemental Figure 10F). In addition, NTP significantly promoted erastin-induced cell death, which could be rescued by the ferroptosis inhibitor Ferr-1, indicating that the treatment of NTP could also stimulate ferroptosis (Figure 12J and Supplemental Figure 10G). Consequently, the treatment of NTP sensitized the IR-resistant lung cancer cells to irradiation as compared to those cells treated with the vehicle (Figure 12K). Altogether, our data suggest that inhibition of RBMS1 by NTP sensitizes IR-resistant lung cancer cells to radiotherapy, providing a novel and effective therapeutic agent for lung cancer patients by promoting ferroptosis.

Discussion

Ferroptosis could be regulated by a variety of factors, thus to participate in regulating cancer progression. However, few studies have shown that RNA binding proteins play vital roles in ferroptosis regulation. For example, DAZAP1 was identified to bind the 3′-UTR of *SLC7A11* mRNA and positively modulate its stability to inhibit ferroptosis (40). The RNA-binding protein ZFP36/TTP protects against ferroptosis by regulating autophagy signaling pathway in hepatic stellate cells (41). Using an shRNA library of RNA binding proteins, we systematically identified that multiple RBPs could control ferroptosis, including RBMS1, SRSF9, TIAL1, PPIG, XRCC6, and etc. al. Specifically, we revealed a model in which the RNA binding protein RBMS1 plays an important regulatory role in mediating ferroptosis, thereby controlling lung cancer progression. We demonstrated that RBMS1 binds to the eIF3d complex to bridge the 3′- and 5′-UTR of *SLC7A11*, which in turn promotes the translation of *SLC7A11*. Subsequently, the increased SLC7A11 inhibits ferroptosis and confers the radioresistance to lung cancer cells to irradiation (Figure 12L). However, when RBMS1 is depleted, the *SLC7A11* mRNA and eIF3d will be released, resulting in the suppression of *SLC7A11* translation. The reduced SLC7A11 promotes ferroptosis, thereby inhibiting lung cancer progression and sensitizing resistant cancer cells to radiotherapy (Figure 12L). Taken together, our data establish RBMS1 as a ferroptosis regulator with therapeutic potentials and clinical values as a prognostic factor.

The RNA binding protein RBMS1 contains two RNA Recognition Motifs (RRMs), and was previously reported to bind directly to the C-terminal portion of *c-Myc*, stimulating the cooperative transforming activity of c-Myc with Ras (42). In addition, as

a posttranscriptional regulator of RNA stability, RBMS1 was shown to bind the 3′-UTR of target mRNAs, leading to increased mRNA stability (33). Functional study of RBMS1 revealed that RBMS1 silencing accompanies colorectal cancer progression in cell line and PDX models as well as clinical samples (33). However, our study demonstrated that the level of RBMS1 is markedly increased in lung cancer patient samples as compared to adjacent normal tissues, and loss of RBMS1 inhibits lung cancer progression in cultured cancer cells, xenograft mice, and genetically conditional knockout mice model. This might be determined by the tissue specificity and distinct localizations of RBMS1, which is similar to the function of *PTEN* (43, 44). Most importantly, we revealed that, instead of regulating mRNA stability, RBMS1 modulates the translation of *SLC7A11*, establishing a novel role of RBMS1 in cancer progression regulation.

As a critical regulator of ferroptosis, SLC7A11 could promote cancer progression partly through inhibiting ferroptosis. For example, the P53 mutant (3KR) retained its tumor-suppressive function partially by inhibiting SLC7A11 expression and inducing ferroptosis (8); SLC7A11 can also promote tumor development by directly interacting with ALOX12 and suppressing ALOX12-mediated ferroptosis in the absence of P53 (45); BAP1 inhibited cancer progression partly by triggering ferroptosis upon SLC7A11 repression (46). Meanwhile, the level of SLC7A11 could be regulated from distinct layers. Both p53 and BAP1 could regulate *SLC7A11* at the transcriptional level (8, 46). The DUB OTUB1 deubiquitinates and stabilizes SLC7A11 protein by post-translational regulation (24). However, the translational regulation of *SLC7A11* remains largely unknown. In our study, for the first time, we reported that RBMS1 binds to eIF3d complex to bridge the 3′- and 5′-UTR of *SLC7A11*, which in turn promotes its translation.

We revealed that loss of RBMS1 repressed the expression of SLC7A11 to stimulate ferroptosis.

In addition to RBMS1, we also identified some other RNA binding proteins that could regulate ferroptosis, including SRSF9, TIA1, XRCC6, and so on. Several identified RBPs have been previously demonstrated to play critical roles in cancer progression. For instance, the RNA binding protein SRSF9 was reported to promote Wnt signaling-mediated tumorigenesis by enhancing beta-catenin biosynthesis (47). Deregulated RNA-binding of TIA1 promotes COX2 expression in colon cancer (48). XRCC6 directly interacts with Mcl1 to stabilize Mcl1, leading to suppression of apoptosis in lung cancer cells (49). However, it still remains largely elusive whether these RNA binding proteins could participate in cancer progression regulation through controlling ferroptosis. Therefore, we will further mechanistically study the functions of such RBPs in mediating ferroptosis, providing novel potential targets for cancer therapeutics in the future.

Methods

Reagents

Erastin was obtained from AbMole (M2679). TBH and ferrostatin-1 were obtained from Sigma-Aldrich (458139 and SML0583). Z-VAD-fmk, 3-Methyladenine, Liproxstatin-1, and NAC were obtained from Selleck (S7023, S2767, S7699 and S1623).

Cell culture

A549, NCI-H1299, HEK293T cells were purchased from the American Type Culture Collection (ATCC). All of the cells were cultured under standard culture conditions (37 °C, 5% CO_2) in culture medium recommended by the ATCC. To generate RBMS1 overexpression or knockdown stable cell lines, HEK293T cells were transfected with either pCDH-Flag-RBMS1 or pLKO.1 RBMS1 constructs, together with pPAX2 and pMD2 lentiviral packaging systems using Sage LipoPlus reagent (Sage) according to the manufacturer's instructions. Viruses were collected at 72 h after transfection and then used to infect A549 and NCI-H1299 cells with Polybrene (8 μg/mL, Sigma) for 24h. Then stably integrated cells were selected by 5μg/mL puromycin for 5 days. To generate doxorubicin (Dox)-inducible RBMS1 knockdown stable cell line, pLKO-Tet-On-RBMS1-shRNA was transfected into HEK293T cells together with pPAX2 and pMD2 lentiviral packaging systems using Sage LipoPlus reagent (Sage) according to the manufacturer's instructions. Viruses were harvested at 72 h after transfection. A549 and NCI-H1299 cells were infected for 24h followed by Puromycin (5 ug/ml) selection. For CRISPR Knockout cells construction, sgRNA was constructed into the lentiCRISPRv2 vector, and package the lentivirus, infected cells with the lentivirus, screened with puromycin to obtain the stable cell line. In the experiment of Cystine deletion, fresh DMEM was used as the control, and the condition DMEM (21013024, gibco) with 1 mM Sodium Pyruvate, 0.2 mM L-Methionine, 4 mM L-Glutamate and 10% FBS was used as low Cystine treatment.

Plasmid construction

To generate the mammalian expression plasmid pCDH-Flag-RBMS1, pCDH-Flag-SLC7A11 and pCDH-Flag-eIF3d, Human RBMS1, SLC7A11 and eIF3d cDNA were

PCR amplified and then cloned into the lentivirus vector pCDH-CMV-MCS-EF1-Puro with N-terminal Flag tag with restriction enzymes *Nhe* I and *Not* I. shRNAs targeting RBMS1 were cloned into pLKO.1 plasmid and pLKO-Tet-On inducible vector. For bacteria protein expression of human eIF3d, eIF3i and eIF3m that express N-terminal His-fused proteins, the cDNAs of eIF3d, eIF3i or eIF3m were inserted into pET-28a(+) with *EcoR* I/*Not* I sites. For expression of recombinant RBMS1 proteins, RBMS1 cDNA was cloned into the pGEX4T1-GST vector with *EcoR* I/*Not* I sites. To generate SLC7A11 luciferase reporter, the DNA fragment of human SLC7A11 gene promoter and 5′-UTR (-679/+ 280) was amplified by PCR and sub-cloned into the *Nhe* I/*Bgl* II sites of the pGL3 enhancer vector (SLC7A11-fluc-T1). All constructs were confirmed by DNA sequencing. Primers for PCR amplification, gRNAs, and shRNAs are listed in Supplementary Table 2.

Cell viability and cell death assays

For cell viability assay, cells were seeded in 96-well plates and treated with drugs for an appropriate time in the next day. Then, remove the medium with drugs and replace with fresh medium containing 10% Cell Counting Kit-8 (CCK8) reagent (APExBIO). After incubation for 2h at 37°C, the plate was analyzed using an enzyme-labeled instrument (DNM-9602, Perlong） and absorbance of the wells was measured at 450 nm. In order to detect cell death, cells were seeded in 12-well plates, and treated with drugs for an appropriate time to induce cell death in the next day. Cells were digested with trypsin to obtain cell precipitation and suspended with PBS. Mix 100 μL cell suspension and 200 μL 0.02% trypan blue together and stain for 1 min, then count the cells with Countess II FL automated cell counter (Thermo Fisher) to get the proportion of dead cells. Or suspended cells with 500 μL PBS containing 5 μL PI (propidium iodide, KGA214, KeyGEN BioTECH). After staining for 15min, the proportion of dead cells was analyzed by a BD Accuri C6 Plus personal flow cytometer (BD Biosciences).

GSH assay

GSH levels was measured by GSH-Glo Glutathione Assay (Promega) kit. In short, seed 6000 cells per well in 96-well plates. The medium was removed in the next day, and add

100 μL 1×GSH-GLO Reagent in each well. Incubate 30 minutes at room temperature. Then add 100 μL reconstituted Luciferin Detection Reagent in every well and mix gently, incubation at room temperature for 15 min. Luminescence was detected by a multifunctional enzyme label analyzer (Enspire2300, Perkin Elmer).

Lipid peroxidation assay

Cells were seeded in the six-well plate and treated with drugs for an appropriate time in the next day, then treated with 5 μM BODIPY 581/591 C11(D3861, Thermo Fisher) and incubated at 37 °C for 30 min. Then wash the cells twice with 1mL 1×PBS, digest cells with trypsin to obtain cell precipitation and suspended with 500 μL PBS. Use BD Accuri C6 Plus personal flow cytometer (BD Biosciences) to analysis changes in fluorescence.

^{13}C-Cystine labelling experiments

The RBMS1 stable knockdown or pLKO.1 control H1299 cells were plated onto 60 mm dishes for 12h. Cells were incubated in the fresh DMEM (21013024, gibco) with 1 mM Sodium Pyruvate, 0.2 mM L-Methionine, 4 mM L-Glutamate for 4h. The medium was then replaced by fresh DMEM (without cystine) supplemented with 0.2 mM L-cystine (3,3′-^{13}C2) (Cambridge Isotope Laboratories, CLM-520-PK) for 4h. Cells were quickly washed for three times with PBS to remove contaminations from the media. The PBS was thoroughly aspirated and cells were immediately quenched in liquid nitrogen and then stored at -80 °C for GC-MS analysis. Protein concentrations were determined by processing a parallel six-well plates and used to normalize metabolite fractions.

Light microscopy and immunofluorescence microscopy

For light microscopy, cells were cultured in 6-well plates and treated with reagents as indicated. Phase contrast images were captured using a Leica microscope equipped with a 10× phase contrast objective. For immunofluorescence microscopy, Cells with stable transfection of pCDH-FLAG-RBMS1 plasmid seeded on glass slides were cultured for 24h to ensure growing well. And after removing medium with PBS, cells were fixed with 4% paraformaldehyde for 20 min followed by washing with PBS for 5min three times, and blocked with 3% BSA in PBS for 10min. Then cells were incubated with primary

antibodies anti-FLAG (Sigma, F3165, 1:100) and anti-Calnexin (Cell Signaling Technology, 2679s, 1:100) overnight at 4°C and then washed with PBS for 5 min three times. Next, the fluorescent-labeled secondary antibodies were used to combine with primary antibodies for 1 h at RT and removed by PBS for 5min three times and then nuclei were labelled with DAPI. Finally, Target proteins with fluorescence were detected by Leica microscope (Leica Mi8, Oil Immersion Objective).

Transmission electron microscopy

For ultrastructural analysis of mitochondria, transmission electron microscopy (TEM) was used. RBMS1 stably depleted or control H1299 cells were treated with or without 5 μM erastin, and fixed with 2.5% glutaraldehyde in 0.1 M PBS (pH 7.4) at 4 °C for 2.5 h, washed three times with 0.1 M PBS and post-fixed in 1% OsO_4 for 2 h at 4 °C. The samples were then dehydrated through an ethanol gradient and subsequently embedded in Spurr's resin. Ultrathin sections were then collected and stained with either uranyl acetate or lead citrate and examined by a JEOL 1200EX transmission electron microscope.

Structured Illumination Microscopy (SIM)

Cells were incubated with Rho123 (2 μM) at 37°C, 5%CO_2 for 2 hours to stain the mitochondria. Subsequently, cells were washed with 1 ml RPMI-1640 medium contained 10% FBS twice and imaged under SIM (Nikon N-SIM Ti-2E). Super-resolution images were performed by Nikon N-STORM/SIM 5.0 Super-Resolution Microscope System with a motorized inverted microscope ECLIPSE Ti2-E, a 100 × / NA 1.49 oil immersion TIRF objective lens (CFI HP), LU-NV series laser unit, and an ORCA-Flash 4.0 SCMOS camera (Hamamatsu Photonics K.K.).

RNA isolation and RT–qPCR

RNA was extracted from cells or RNA immunoprecipitation samples using Trizol reagent (Invitrogen) according to the manufacturer's instructions. Genome DNAs were removed by 30 min DNase I (Promega M6101) treatment at 37 °C. Then add equal volumes Stop Solution to terminate the reaction and incubate at 65 °C for 10 min to inactive the DNase. Total RNA (2 μg) was then reverse-transcribed with PrimeScript RT reagent kit (Takara)

with random primer. We performed the real-time PCR using the Maxima SYBR Green qPCR Master Mix (Thermo Scientific) and a 7500 real-time PCR system (Life Technologies) according to manufacturer's instructions.

Statistics

Data are presented as mean ± SEM. Statistical significance was determined by Student's two-tailed t-test, One-way ANOVA with Dunnett multiple comparisons, One-way repeated measures ANOVA, and One-way ANOVA with Tukey's multiple comparisons according to different situation.

Study Approval

The Institutional Animal Care and Use Committee of the Dalian Medical University approved use of animal models in this study.

All human tumor tissues were obtained with written informed consent from patients or their guardians prior to participation in the study. The Institutional Review Board of the Dalian Medical University approved use of the tumor specimens in this study.

Data Availability

Ribo-seq data in this study have been deposited in Gene Expression Omnibus of NCBI with the accession code GSE171640. The authors declare that all the data supporting the findings of this study are available within the article and its Supplemental information files.

Author contributions

YW conceived the project and designed the experiments. WZ, YS, LB, LZ, YY, QZ, YQ, WG, WH, LW, HC, QQ, JZ, YY, and CP designed and performed most of the

experiments, whereas CC, DC, SF, HP, ZX, JZ, SZ, XL, HL, and QL performed data analysis. YW provided funds. YW and XL wrote the manuscript.

Acknowledgements

This work was supported by the National Natural Science Foundation of China (81830088, 81422038, 91540110, and 31471235 to YW; 81872247 and 31400726 to W Z); Liaoning Revitalization Talents Program XLYC1802067 to YW; the Department of Science and Technology of Liaoning Province (2021JH6/10500160 to YW); the Newton Advanced Fellowship from the Academy of Medical Sciences in UK (JXR11831 to YW); Dalian High Level Talents Renovation Supporting Program (2019RQ097 to WZ); the Youth Innovation Promotion Association CAS (2019267 to YY).

References:

1. Dixon SJ, Lemberg KM, Lamprecht MR, Skouta R, Zaitsev EM, Gleason CE, et al. Ferroptosis: an iron-dependent form of nonapoptotic cell death. *Cell.* 2012;149(5):1060-72.
2. Yang WS, and Stockwell BR. Ferroptosis: Death by Lipid Peroxidation. *Trends Cell Biol.* 2016;26(3):165-76.
3. Xie Y, Hou W, Song X, Yu Y, Huang J, Sun X, et al. Ferroptosis: process and function. *Cell Death Differ.* 2016;23(3):369-79.
4. Tang D, Chen X, Kang R, and Kroemer G. Ferroptosis: molecular mechanisms and health implications. *Cell Res.* 2021;31(2):107-25.
5. Chen X, Kang R, Kroemer G, and Tang D. Broadening horizons: the role of ferroptosis in cancer. *Nat Rev Clin Oncol.* 2021.
6. Zhu S, Zhang Q, Sun X, Zeh HJ, 3rd, Lotze MT, Kang R, et al. HSPA5 Regulates Ferroptotic Cell Death in Cancer Cells. *Cancer Res.* 2017;77(8):2064-77.
7. Zhang Y, Shi J, Liu X, Feng L, Gong Z, Koppula P, et al. BAP1 links metabolic regulation of ferroptosis to tumour suppression. *Nat Cell Biol.* 2018;20(10):1181-92.
8. Jiang L, Kon N, Li T, Wang SJ, Su T, Hibshoosh H, et al. Ferroptosis as a p53-mediated activity during tumour suppression. *Nature.* 2015;520(7545):57-62.
9. Jennis M, Kung CP, Basu S, Budina-Kolomets A, Leu JI, Khaku S, et al. An African-specific polymorphism in the TP53 gene impairs p53 tumor suppressor function in a mouse model. *Genes Dev.* 2016;30(8):918-30.
10. Roh JL, Kim EH, Jang HJ, Park JY, and Shin D. Induction of ferroptotic cell death for overcoming cisplatin resistance of head and neck cancer. *Cancer Lett.* 2016;381(1):96-103.
11. Tsoi J, Robert L, Paraiso K, Galvan C, Sheu KM, Lay J, et al. Multi-stage Differentiation Defines Melanoma Subtypes with Differential Vulnerability to Drug-Induced Iron-Dependent Oxidative Stress. *Cancer Cell.* 2018;33(5):890-904 e5.
12. Viswanathan VS, Ryan MJ, Dhruv HD, Gill S, Eichhoff OM, Seashore-Ludlow B, et al. Dependency of a therapy-resistant state of cancer cells on a lipid peroxidase pathway. *Nature.* 2017;547(7664):453-7.
13. Hangauer MJ, Viswanathan VS, Ryan MJ, Bole D, Eaton JK, Matov A, et al. Drug-tolerant persister cancer cells are vulnerable to GPX4 inhibition. *Nature.* 2017;551(7679):247-50.
14. Wang W, Green M, Choi JE, Gijon M, Kennedy PD, Johnson JK, et al. CD8(+) T cells regulate tumour ferroptosis during cancer immunotherapy. *Nature.* 2019;569(7755):270-4.
15. Lei G, Zhang Y, Koppula P, Liu X, Zhang J, Lin SH, et al. The role of ferroptosis in ionizing radiation-induced cell death and tumor suppression. *Cell Res.* 2020;30(2):146-62.
16. Lang X, Green MD, Wang W, Yu J, Choi JE, Jiang L, et al. Radiotherapy and Immunotherapy Promote Tumoral Lipid Oxidation and Ferroptosis via Synergistic Repression of SLC7A11. *Cancer Discov.* 2019;9(12):1673-85.

17. Koppula P, Zhuang L, and Gan B. Cystine transporter SLC7A11/xCT in cancer: ferroptosis, nutrient dependency, and cancer therapy. *Protein Cell.* 2020.
18. Koppula P, Zhang Y, Zhuang L, and Gan B. Amino acid transporter SLC7A11/xCT at the crossroads of regulating redox homeostasis and nutrient dependency of cancer. *Cancer Commun (Lond).* 2018;38(1):12.
19. Yang WS, SriRamaratnam R, Welsch ME, Shimada K, Skouta R, Viswanathan VS, et al. Regulation of ferroptotic cancer cell death by GPX4. *Cell.* 2014;156(1-2):317-31.
20. Friedmann Angeli JP, Schneider M, Proneth B, Tyurina YY, Tyurin VA, Hammond VJ, et al. Inactivation of the ferroptosis regulator Gpx4 triggers acute renal failure in mice. *Nat Cell Biol.* 2014;16(12):1180-91.
21. Conrad M, and Sato H. The oxidative stress-inducible cystine/glutamate antiporter, system x (c) (-) : cystine supplier and beyond. *Amino Acids.* 2012;42(1):231-46.
22. Rojo de la Vega M, Chapman E, and Zhang DD. NRF2 and the Hallmarks of Cancer. *Cancer Cell.* 2018;34(1):21-43.
23. Badeaux AI, and Shi Y. Emerging roles for chromatin as a signal integration and storage platform. *Nat Rev Mol Cell Biol.* 2013;14(4):211-24.
24. Liu T, Jiang L, Tavana O, and Gu W. The Deubiquitylase OTUB1 Mediates Ferroptosis via Stabilization of SLC7A11. *Cancer Res.* 2019;79(8):1913-24.
25. Ishimoto T, Nagano O, Yae T, Tamada M, Motohara T, Oshima H, et al. CD44 variant regulates redox status in cancer cells by stabilizing the xCT subunit of system xc(-) and thereby promotes tumor growth. *Cancer Cell.* 2011;19(3):387-400.
26. Li F, Zhao H, Su M, Xie W, Fang Y, Du Y, et al. HnRNP-F regulates EMT in bladder cancer by mediating the stabilization of Snail1 mRNA by binding to its 3' UTR. *EBioMedicine.* 2019;45:208-19.
27. Wang Y, Chen D, Qian H, Tsai YS, Shao S, Liu Q, et al. The splicing factor RBM4 controls apoptosis, proliferation, and migration to suppress tumor progression. *Cancer Cell.* 2014;26(3):374-89.
28. Chen TM, Lai MC, Li YH, Chan YL, Wu CH, Wang YM, et al. hnRNPM induces translation switch under hypoxia to promote colon cancer development. *EBioMedicine.* 2019;41:299-309.
29. Boise LH, Gonzalez-Garcia M, Postema CE, Ding L, Lindsten T, Turka LA, et al. bcl-x, a bcl-2-related gene that functions as a dominant regulator of apoptotic cell death. *Cell.* 1993;74(4):597-608.
30. Warzecha CC, Sato TK, Nabet B, Hogenesch JB, and Carstens RP. ESRP1 and ESRP2 are epithelial cell-type-specific regulators of FGFR2 splicing. *Mol Cell.* 2009;33(5):591-601.
31. Zhou L, Guo J, and Jia R. Oncogene SRSF3 suppresses autophagy via inhibiting BECN1 expression. *Biochem Biophys Res Commun.* 2019;509(4):966-72.
32. Kimura K, Saga H, Hayashi K, Obata H, Chimori Y, Ariga H, et al. c-Myc gene single-strand binding protein-1, MSSP-1, suppresses transcription of alpha-smooth muscle actin gene in chicken visceral smooth muscle cells. *Nucleic Acids Res.* 1998;26(10):2420-5.

33. Yu J, Navickas A, Asgharian H, Culbertson B, Fish L, Garcia K, et al. RBMS1 Suppresses Colon Cancer Metastasis through Targeted Stabilization of Its mRNA Regulon. *Cancer Discov.* 2020;10(9):1410-23.
34. Van Nostrand EL, Freese P, Pratt GA, Wang X, Wei X, Xiao R, et al. A large-scale binding and functional map of human RNA-binding proteins. *Nature.* 2020;583(7818):711-9.
35. Mao C, Liu X, Zhang Y, Lei G, Yan Y, Lee H, et al. DHODH-mediated ferroptosis defence is a targetable vulnerability in cancer. *Nature.* 2021;593(7860):586-90.
36. Lee AS, Kranzusch PJ, Doudna JA, and Cate JH. eIF3d is an mRNA cap-binding protein that is required for specialized translation initiation. *Nature.* 2016;536(7614):96-9.
37. Shi Y, Liu N, Lai W, Yan B, Chen L, Liu S, et al. Nuclear EGFR-PKM2 axis induces cancer stem cell-like characteristics in irradiation-resistant cells. *Cancer Lett.* 2018;422:81-93.
38. Cui B, Luo Y, Tian P, Peng F, Lu J, Yang Y, et al. Stress-induced epinephrine enhances lactate dehydrogenase A and promotes breast cancer stem-like cells. *J Clin Invest.* 2019;129(3):1030-46.
39. Shin SE, Li H, Kim HS, Kim HW, Seo MS, Ha KS, et al. Nortriptyline, a tricyclic antidepressant, inhibits voltage-dependent K(+) channels in coronary arterial smooth muscle cells. *Korean J Physiol Pharmacol.* 2017;21(2):225-32.
40. Wang Q, Guo Y, Wang W, Liu B, Yang G, Xu Z, et al. RNA binding protein DAZAP1 promotes HCC progression and regulates ferroptosis by interacting with SLC7A11 mRNA. *Exp Cell Res.* 2021;399(1):112453.
41. Zhang Z, Guo M, Li Y, Shen M, Kong D, Shao J, et al. RNA-binding protein ZFP36/TTP protects against ferroptosis by regulating autophagy signaling pathway in hepatic stellate cells. *Autophagy.* 2020;16(8):1482-505.
42. Niki T, Izumi S, Saegusa Y, Taira T, Takai T, Iguchi-Ariga SM, et al. MSSP promotes ras/myc cooperative cell transforming activity by binding to c-Myc. *Genes Cells.* 2000;5(2):127-41.
43. Kim SK, Su LK, Oh Y, Kemp BL, Hong WK, and Mao L. Alterations of PTEN/MMAC1, a candidate tumor suppressor gene, and its homologue, PTH2, in small cell lung cancer cell lines. *Oncogene.* 1998;16(1):89-93.
44. Xie P, Peng Z, Chen Y, Li H, Du M, Tan Y, et al. Neddylation of PTEN regulates its nuclear import and promotes tumor development. *Cell Res.* 2021;31(3):291-311.
45. Chu B, Kon N, Chen D, Li T, Liu T, Jiang L, et al. ALOX12 is required for p53-mediated tumour suppression through a distinct ferroptosis pathway. *Nat Cell Biol.* 2019;21(5):579-91.
46. Zhang Y, Zhuang L, and Gan B. BAP1 suppresses tumor development by inducing ferroptosis upon SLC7A11 repression. *Mol Cell Oncol.* 2019;6(1):1536845.
47. Fu Y, Huang B, Shi Z, Han J, Wang Y, Huangfu J, et al. SRSF1 and SRSF9 RNA binding proteins promote Wnt signalling-mediated tumorigenesis by enhancing beta-catenin biosynthesis. *EMBO Mol Med.* 2013;5(5):737-50.

48. Dixon DA, Balch GC, Kedersha N, Anderson P, Zimmerman GA, Beauchamp RD, et al. Regulation of cyclooxygenase-2 expression by the translational silencer TIA-1. *J Exp Med.* 2003;198(3):475-81.
49. Wang B, Xie M, Li R, Owonikoko TK, Ramalingam SS, Khuri FR, et al. Role of Ku70 in deubiquitination of Mcl-1 and suppression of apoptosis. *Cell Death Differ.* 2014;21(7):1160-9.

Figures legends

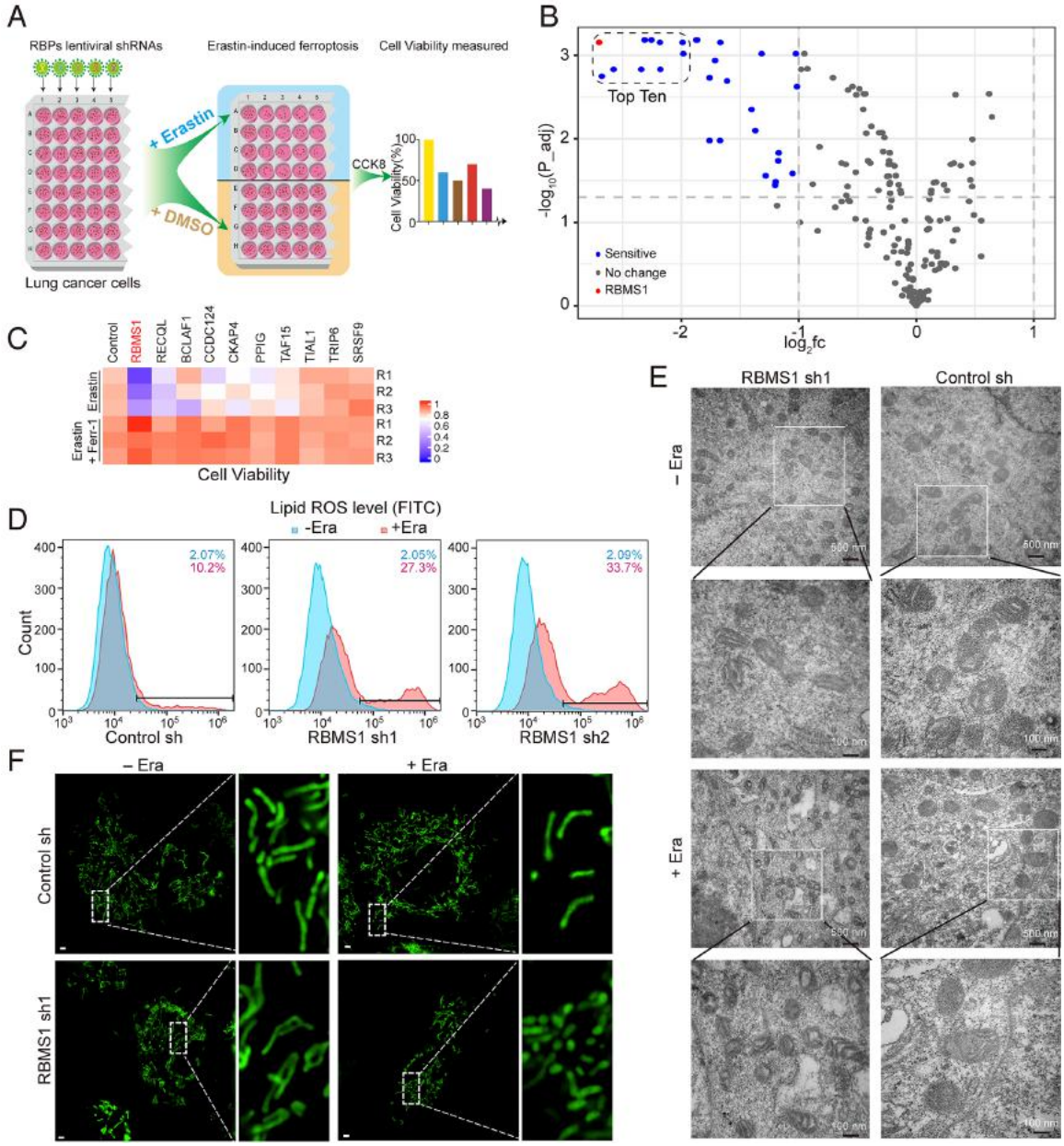

Figure 1 Systematic identification of RBMS1 as a key regulator of ferroptosis in lung cancer. (A) Workflow for RBPs identification in ferroptosis-regulation. A549 cells were infected with 190 shRNAs-viruses for distinct RBPs respectively. **(B)** Volcano-plot illustrating RBPs in regulating ferroptosis. Top-ten candidates are marked. **(C)** Heat-map depicting cell viability of A549 cells with top-ten identified RBPs in (B) depleted using distinct shRNAs with erastin, erastin and Ferrostatin-1 (Ferr-1). **(D)** Lipid-peroxidation

was measured by flow-cytometry after C11-BODIPY-staining in RBMS1-depleted H1299 cells. **(E)** H1299 cells with RBMS1-depletion were treated with erastin and subjected to TEM. Scale bars: left, 500 nm; right, 100 nm. **(F)** RBMS1-depleted H1299 cells were treated with/without erastin and stained with Rho123, a known mitochondria-tracker-probe, and subjected to SIM. Scale bars, 2 μm.

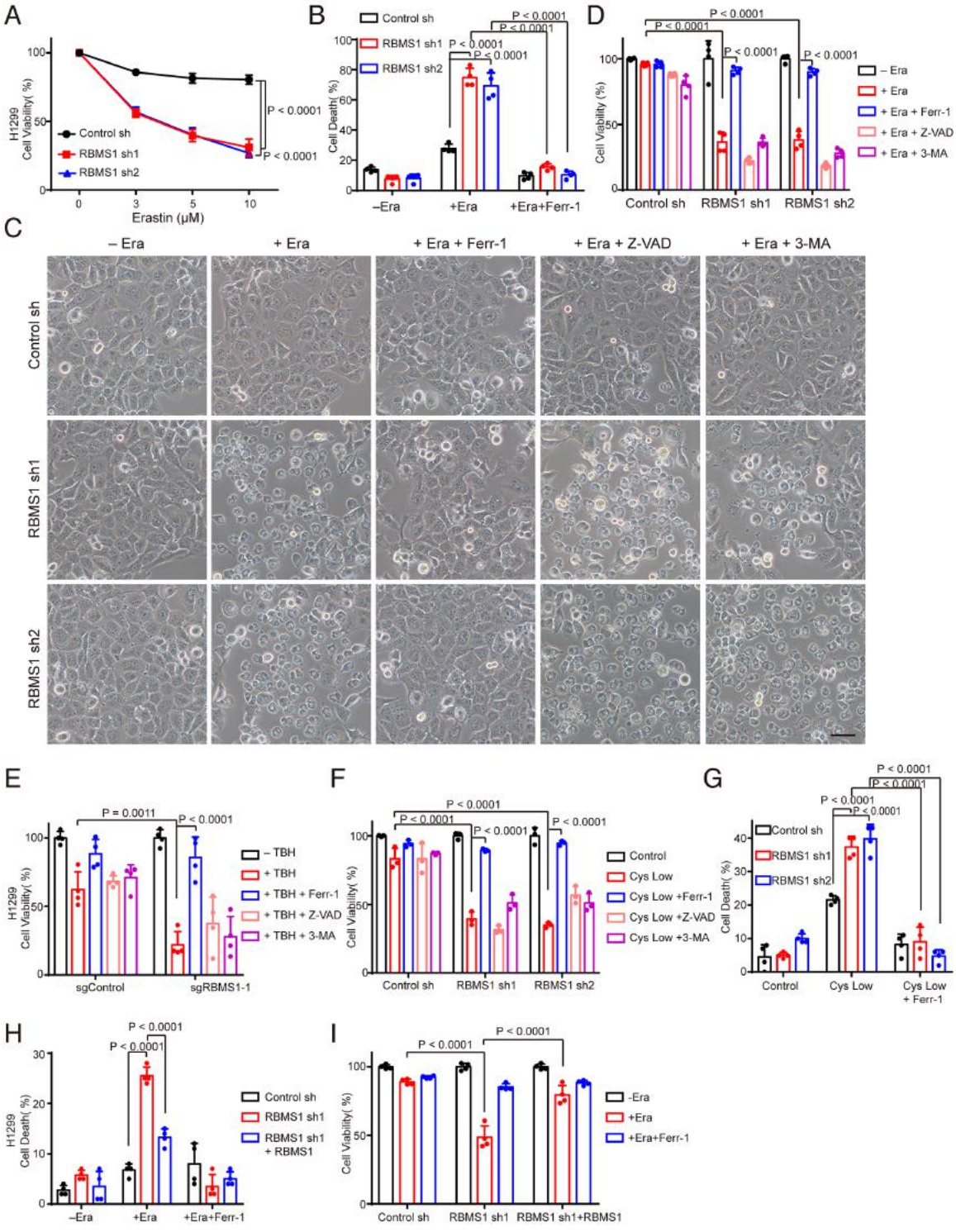

Figure 2 RBMS1 ablation promotes lung cancer cell ferroptosis. (A) Cell viability was assessed after treatment with different concentrations of erastin in RBMS1-depleted H1299 cells. **(B)** Cell death was measured after treatment with erastin (Era), Ferr-1 and

erastin in RBMS1-depleted H1299 cells. **(C)** Representative phase-contrast images of H1299 cells with RBMS1-depletion treated with erastin, erastin and Ferr-1, erastin and Z-VAD-fmk (Z-VAD), erastin and 3-MA, respectively. Scale bars, 100 μm. **(D-E)** Bar graphs showing cell viability in RBMS1-depleted H1299 cells treated with erastin (D) or tert-butyl hydroperoxide (TBH) (E) combined with Ferr-1, Z-VAD, or 3-MA respectively. **(F)** Cell viability of H1299 cells with RBMS1-depletion was measured after culturing in cystine-low-medium combined with Ferr-1, Z-VAD, or 3-MA respectively. **(G)** Bar graph showing cell death of H1299 cells with RBMS1-depletion cultured in cystine-low-medium with/without Ferr-1. **(H-I)** Cell death (H) and viability (I) were measured after treatment with earstin, erastin and Ferr-1 in RBMS1-depleted H1299 cells with/without RBMS1 re-expression. Data represent mean ± SEM, n = 3 (**A**, **F**) or 4 (**B**, **D**, **E**, **G**, **H**, **I**) independent repeats. P values were determined using One-way repeated measures ANOVA in A; One-way ANOVA with Tukey's multiple comparisons in **B**, **D**, **E**, **F**, **G**, **H**, **I**.

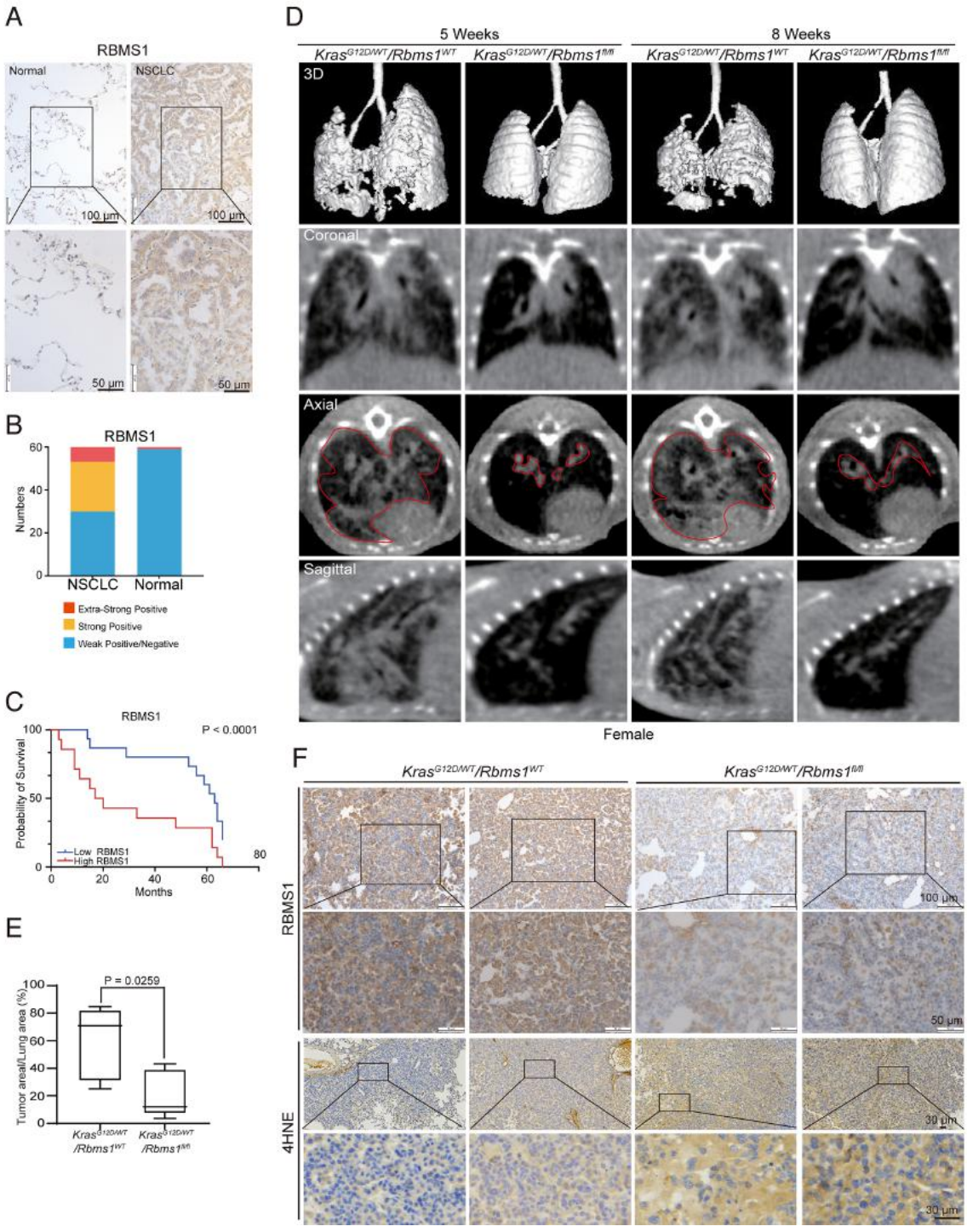

Figure 3 RBMS1 is associated with lung cancer progression and prognosis in humans and mice. (A) Representative images from immunohistochemical staining of RBMS1 in lung cancers (n = 60) and matched adjacent normal tissues (n = 60). Scale

bars are indicated in the pictures. **(B)** The quantification of RBMS1 protein level in lung cancer and adjacent normal lung tissues. The RBMS1 level were respectively classified into three grades (weak positive/negative, strong positive, extra-strong positive) by results from immunohistochemical staining and plotted. **(C)** Kaplan-Meier curve showing overall survival of lung cancers with high or low RBMS1 expression. **(D)** Micro-CT images in indicated planes from female mice with or without RBMS1 deletion (*Kras*$^{G12D/WT}$*/Rbms1*^{WT} or *Kras*$^{G12D/WT}$*/Rbms1*$^{fl/fl}$ CKO) in lung at 5 or 8 weeks post infection of 9×10^{10} vg AAV-GFP-Cre. Three-dimensional rendering of micro-CT data with lungs in gray, lost part represented tumor. The lung tumor areas of *Kras*$^{G12D/WT}$*/Rbms1*^{WT} or *Kras*$^{G12D/WT}$*/Rbms1*$^{fl/fl}$ CKO mice were marked in the Axial plane pictures. Areas within the marked red line were tumor. **(E)** The lung tumor areas of *Kras*$^{G12D/WT}$*/Rbms1*^{WT} or *Kras*$^{G12D/WT}$*/Rbms1*$^{fl/fl}$ CKO mice marked in (D) were calculated. The median, upper and lower quartiles of tumor areas were plotted as box plot (n = 5, P values from unpaired t-test). **(F)** Tumors were removed from *Kras*$^{G12D/WT}$*/Rbms1*^{WT} or *Kras*$^{G12D/WT}$*/Rbms1*$^{fl/fl}$ CKO mice and subjected to immunohistochemical staining with RBMS1 and 4HNE antibodies. The representative images were shown. Scale bars are indicated in the pictures.

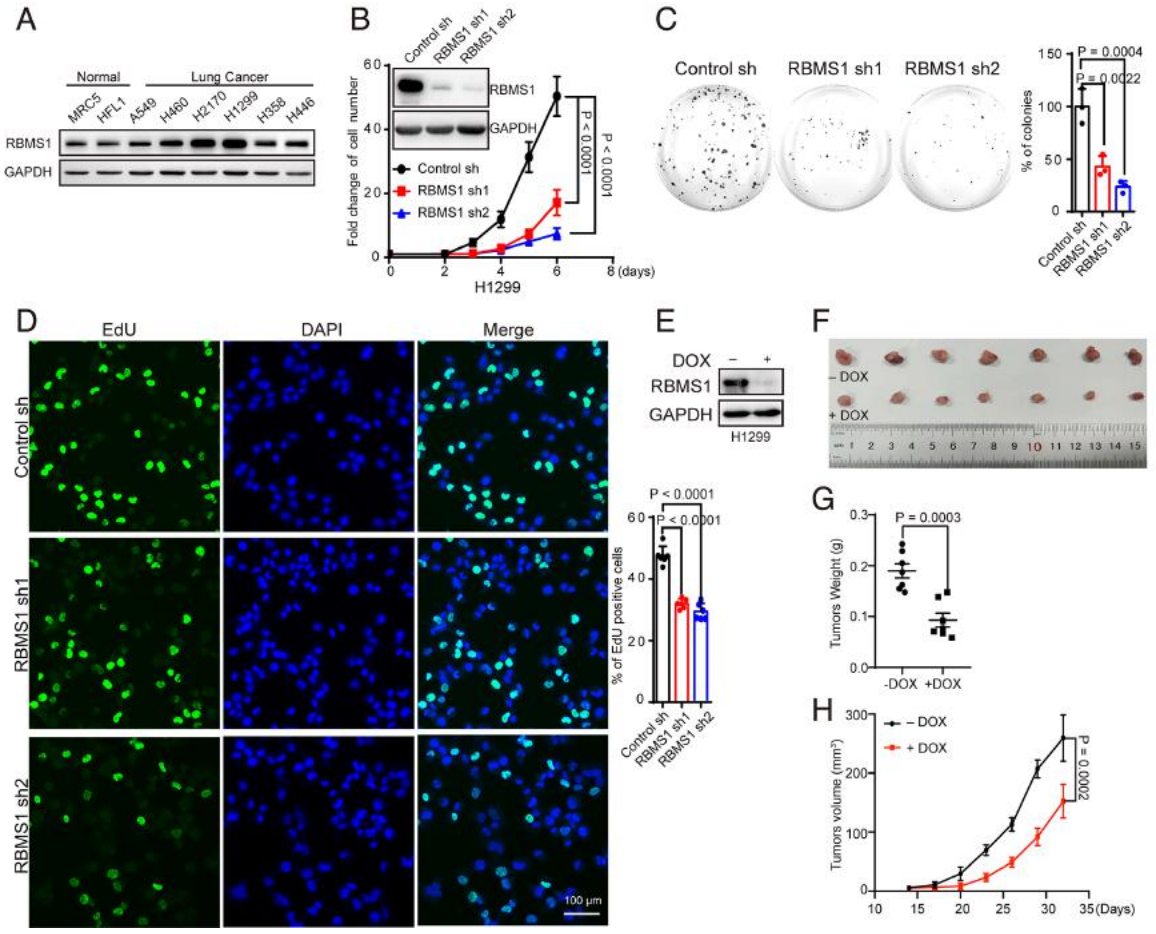

Figure 4 Loss of RBMS1 inhibits lung cancer cell proliferation and progression in vitro and in vivo. (A) Levels of RBMS1 in the indicated lung cancer cell lines and normal bronchial cell lines were measured by a western blot assay. **(B)** H1299 cells with stable depletion of RBMS1 or control were grown for six days, with cell numbers counted every two days. The changes of cell numbers were compared to day 0. The mean ± SEM from three experiments was plotted (P values were determined by One-way repeated measures ANOVA). **(C)** Colony formation assays using H1299 cells with stable depletion of RBMS1. Images of the whole plate are shown. Three experiments were carried out with mean ± SEM of relative colony numbers plotted (P values were determined by One-way ANOVA with Dunnett multiple comparisons). **(D)** The

proliferative abilities of RBMS1 stably depleted H1299 cells were measured with EdU staining assay. Six experiments were conducted with mean ± SEM of percentage of EdU positive cells plotted (P values were determined by One-way ANOVA with Dunnett multiple comparisons). **(E)** The protein levels of RBMS1 in H1299 cells containing doxycycline-induced depletion of RBMS1 were examined in the absence or presence of doxycycline with a western blot assay. **(F-H)** Xenograft tumors were generated using nude mice subcutaneously injected with H1299 cells containing doxycycline-induced depletion of RBMS1. Mice were fed with water containing doxycycline or not. Pictures of the tumors removed after thirty-two days were shown in (F). Tumors were weighed and plotted in (G) (P values were calculated with unpaired t-test). The average sizes of xenograft tumors were measured every three days and plotted in (H) (n = 7, error bars indicate mean ± SEM, P values were determined by One-way repeated measures ANOVA).

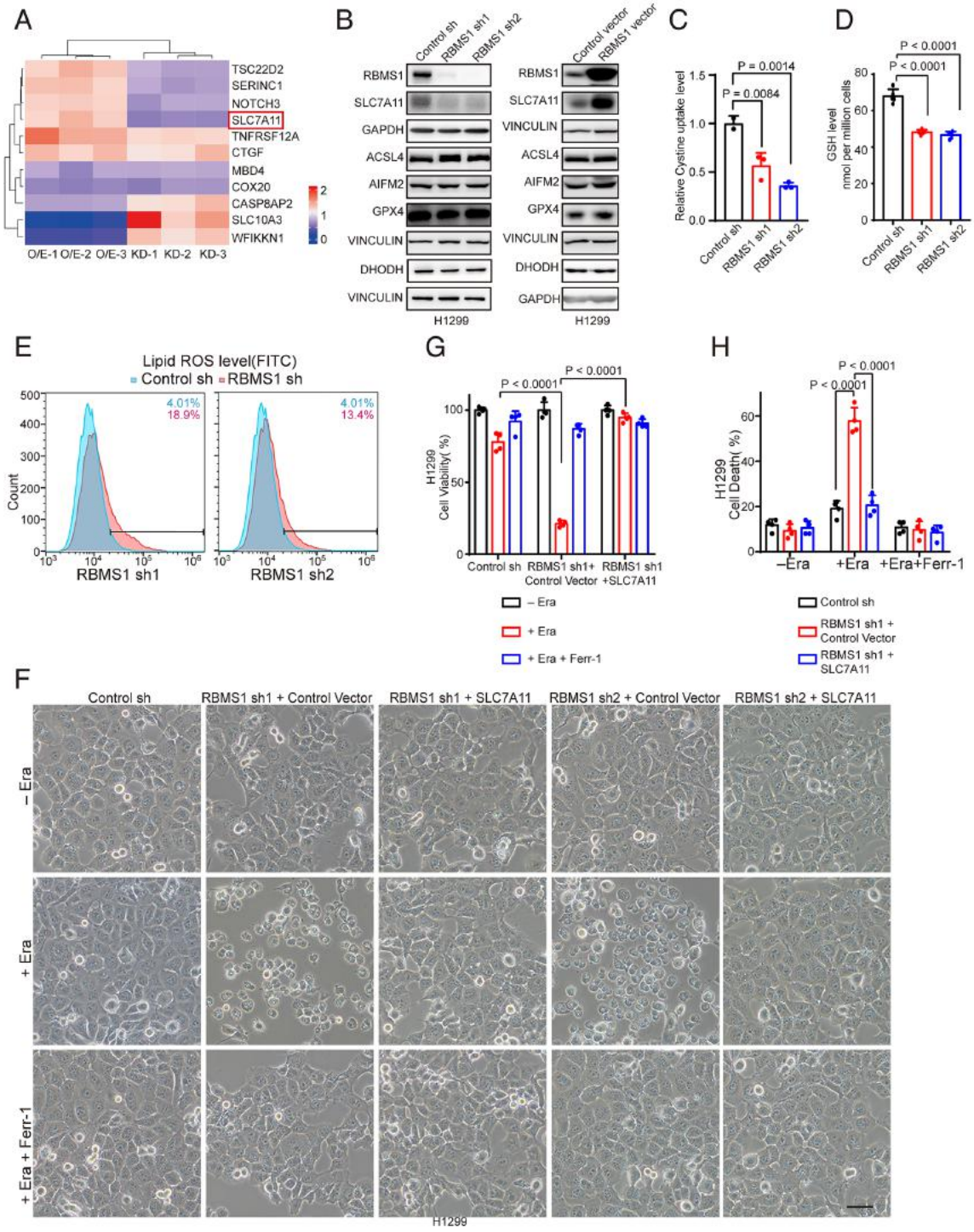

Figure 5 Depleted RBMS1 stimulates ferroptosis through decreased SLC7A11. (A) Heat-map depicting levels of the most differentially expressed RBPs from Quantitative-proteomics using A549 cells with depleted- or overexpressed-RBMS1. **(B)** Levels of

ferroptosis-related genes were examined in RBMS1-depleted or -overexpressed H1299 cells. **(C)** The relative level of cystine-uptake was measured in RBMS1-depleted H1299 cells. **(D)** Bar graph demonstrating intracellular GSH levels in RBMS1-depleted H1299 cells. **(E)** Lipid-peroxidation was measured by flow-cytometry after C11-BODIPY-staining in RBMS1-depleted H1299 cells. **(F)** Representative phase-contrast images of H1299 cells with RBMS1-depletion, with/without SLC7A11 re-expression, treated with erastin, erastin and Ferr-1 respectively. Scale bars, 100 μm. **(G-H)** Bar graphs showing cell viability (G) and death (H) in H1299 cells with RBMS1-knockdown, with/without SLC7A11 re-expression treated with erastin, erastin and Ferr-1. Data represent mean ± SEM, n = 3 (**C**, **D**) or 4 (**G**, **H**), independent repeats. P values were determined by One-way ANOVA with Dunnett multiple comparisons in C, D; One-way ANOVA with Tukey's multiple comparisons in G, H.

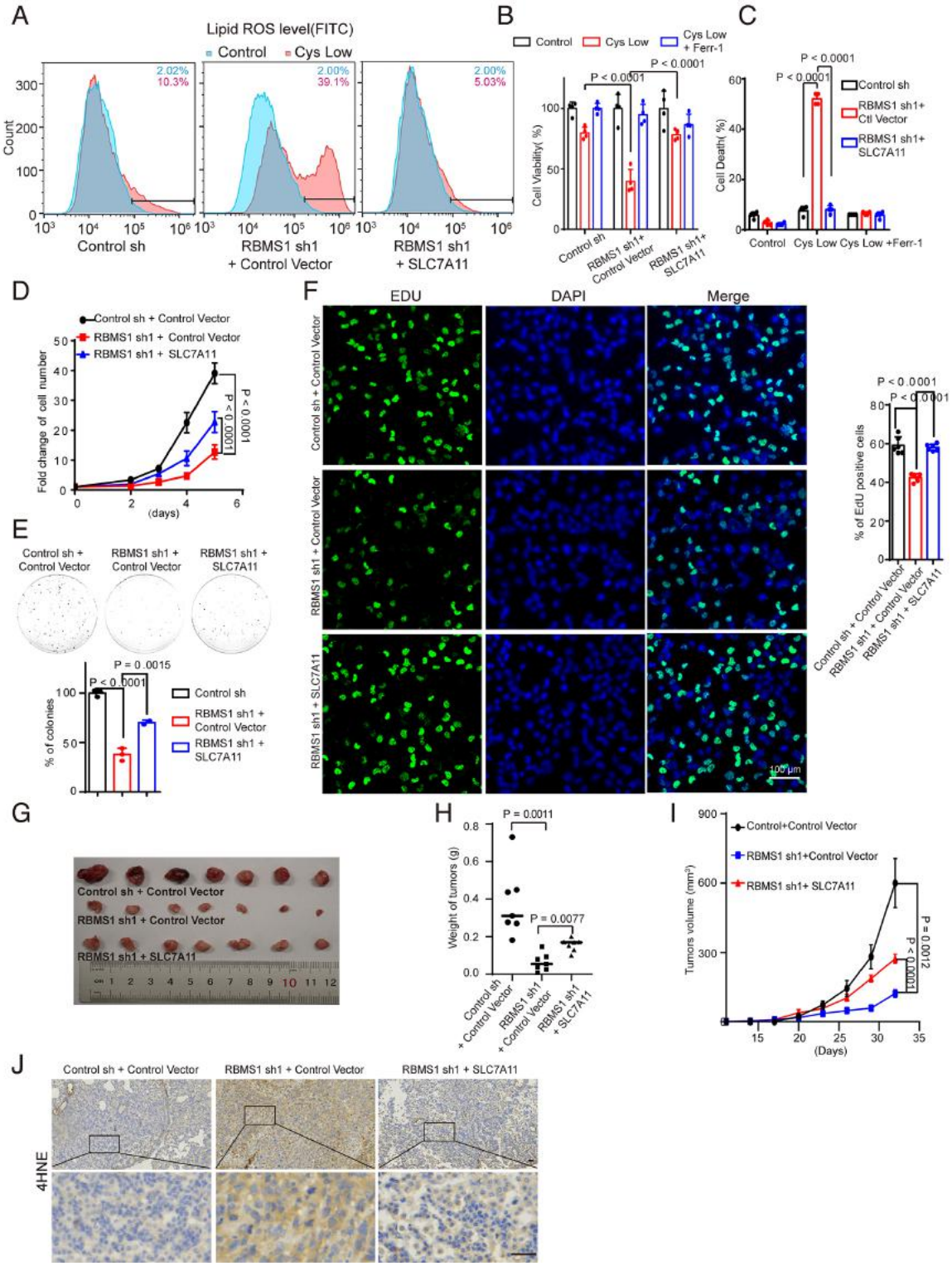

Figure 6 Depletion of RBMS1 inhibits lung cancer progression partially through decreased SLC7A11 and promoting ferroptosis. (A) Lipid-peroxidation was measured

in H1299 cells with RBMS1-depletion, with/without SLC7A11 re-expression, cultured in cystine-low-medium. **(B-C)** Cell viability (B) and death (C) of H1299 cells with RBMS1-depletion, with/without SLC7A11 re-expression, were measured after culturing in cystine-low-medium combined with Ferr-1. **(D-F)** Cell growth (D), colony formation (E), and proliferative abilities (F) of H1299 cells with RBMS1-depletion, with/without SLC7A11 re-expression were measured. **(G-H)** H1299 cells with RBMS1-knockdown, with/without SLC7A11 re-expression were subcutaneously injected into the flank of nude mice. Pictures of the tumors removed were shown in (G). Tumors were weighed and plotted in (H). (**I**) The average sizes of xenograft-tumors were measured (n=7). (**J**) Immunohistochemical-staining of 4-HNE of tumor from H1299 cells with RBMS1-depletion, with/without SLC7A11 re-expression. Scale bars, 30 μm. Data represent mean ± SEM, n = 3 (**D**) or 4 (**B**, **C**), 6 (F) independent repeats. P values were determined by One-way ANOVA with Tukey's multiple comparisons in B, C, E, F, H; and One-way repeated measures ANOVA in D, I.

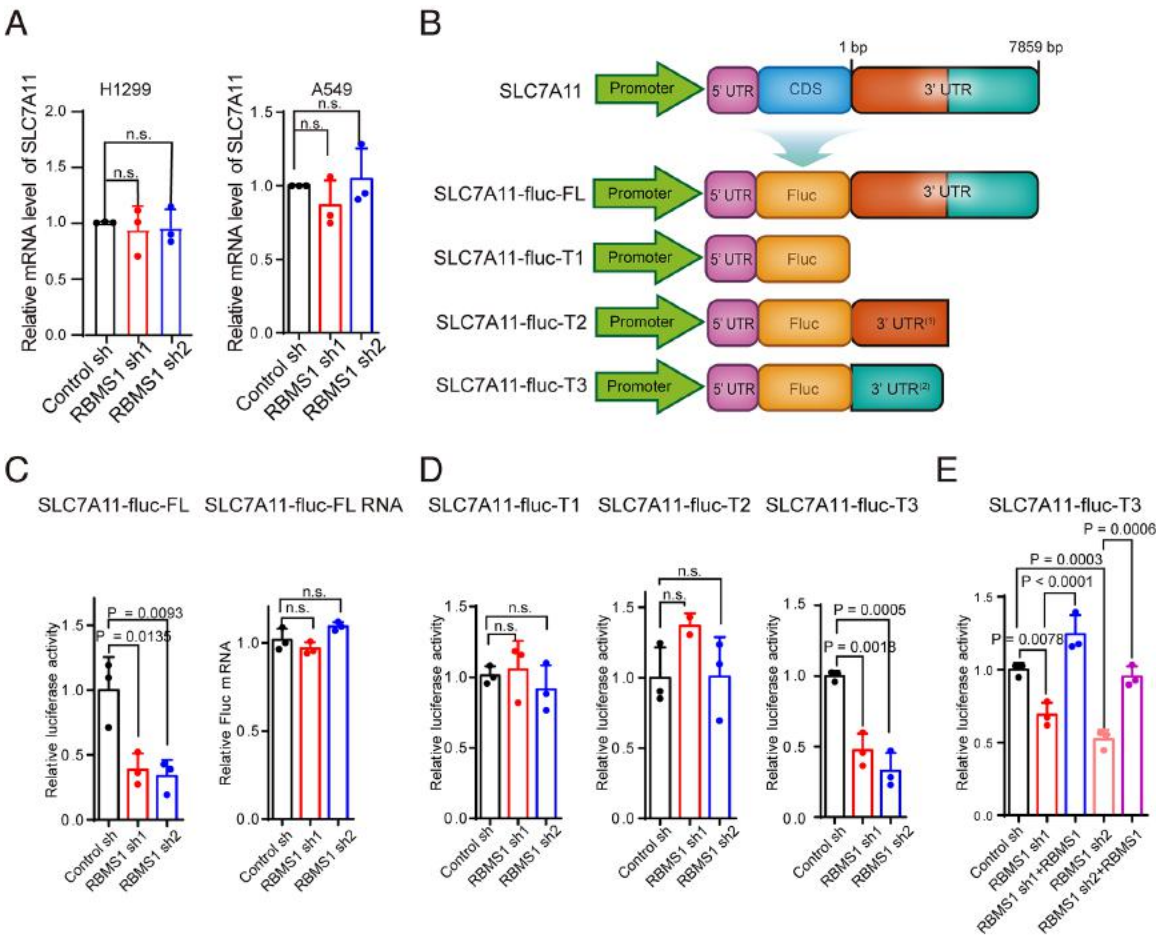

Figure 7 RBMS1 regulates SLC7A11 translation. (**A**) The mRNA levels of SLC7A11 in RBMS1-depleted H1299 and A549 cells were examined using qRT-PCR. (**B**) Schematic of *SLC7A11* luciferase reporter plasmids. SLC7A11-fluc-FL (promoter region, 5′-UTR, and 3′-UTR); SLC7A11-fluc-T1 (promoter region and 5′-UTR); SLC7A11-fluc-T2 (promoter region, 5′-UTR, and 1st-3846th nt region of 3′-UTR); SLC7A11-fluc-T3 (promoter region, 5′-UTR, and 3827th-7859th nt region of 3′-UTR). **(C)** SLC7A11-fluc-FL was transiently transfected into RBMS1-depleted H1299 cells. The relative luciferase activities were determined by calculating the ratio of firefly-luciferase over Renilla-luciferase activities. The mRNA level of SLC7A11-fluc in RBMS1-depleted H1299 cells with transient transfection of SLC7A11-fluc-FL was examined using qRT-PCR. **(D)**

SLC7A11-fluc-T1, SLC7A11-fluc-T2, and SLC7A11-fluc-T3, were transiently transfected into RBMS1-depleted H1299 cells. The relative luciferase activities were determined by calculating the ratio of firefly-luciferase over Renilla-luciferase activities. **(E)** SLC7A11-fluc-T3 was transiently transfected into RBMS1-depleted H1299 cells in the absence or presence of re-expressed RBMS1. The relative luciferase activities were determined by calculating the ratio of firefly-luciferase over Renilla-luciferase activities. Data represent mean ± SEM, n = 3 (A, C, D, E) independent repeats. P values were determined by One-way ANOVA with Dunnett multiple comparisons in A, C, and D; One-way ANOVA with Tukey's multiple comparisons in E.

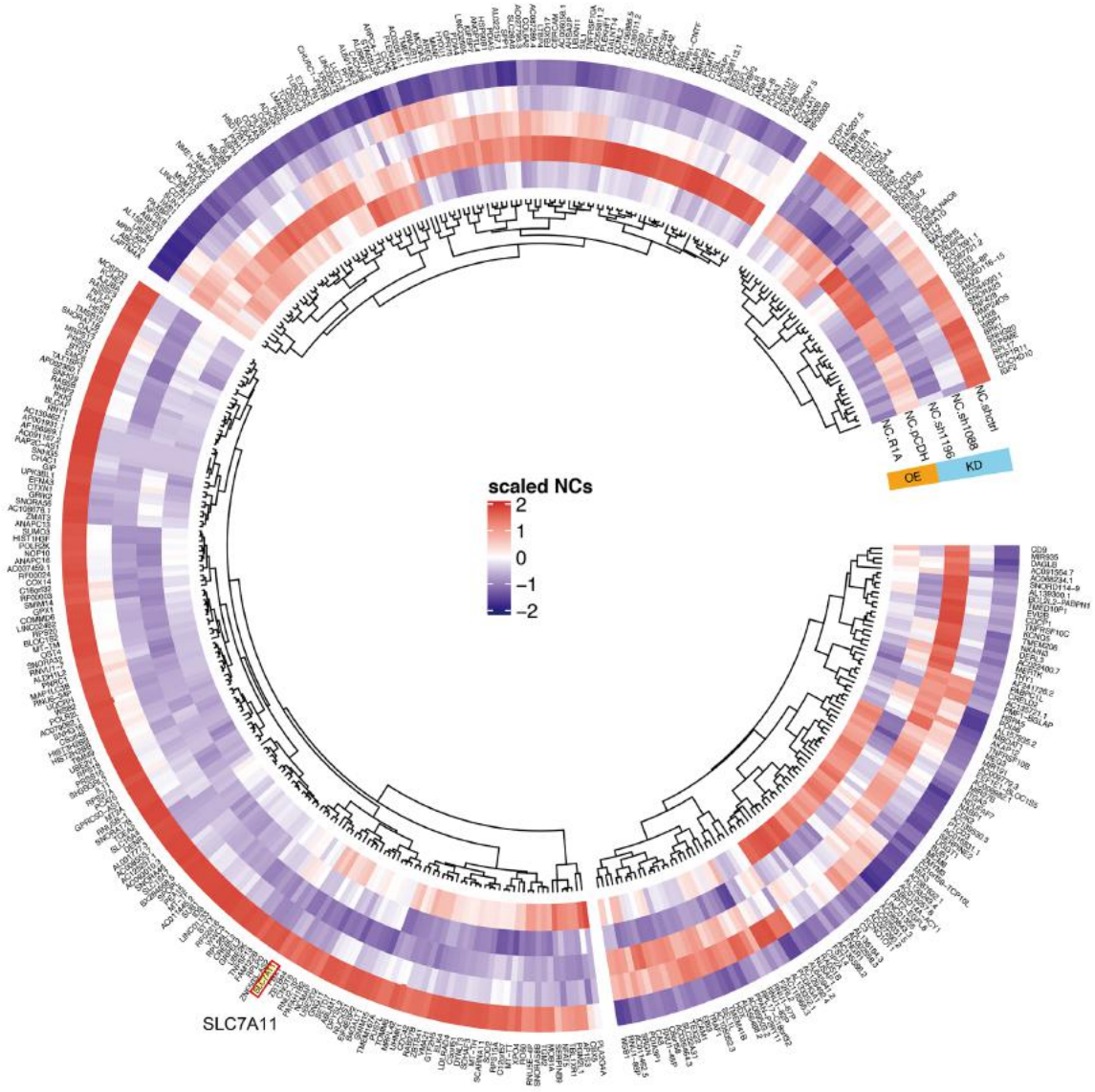

Figure 8 Ribo-seq analysis of RBMS1-depleted or overexpressed cells. Ribo-seq assay was applied with RBMS1-depleted or overexpressed cells. Clustering heatmap of the differentially expressed genes was assessed with the Euclidean distance measurement in column and the Z-normalization in row.

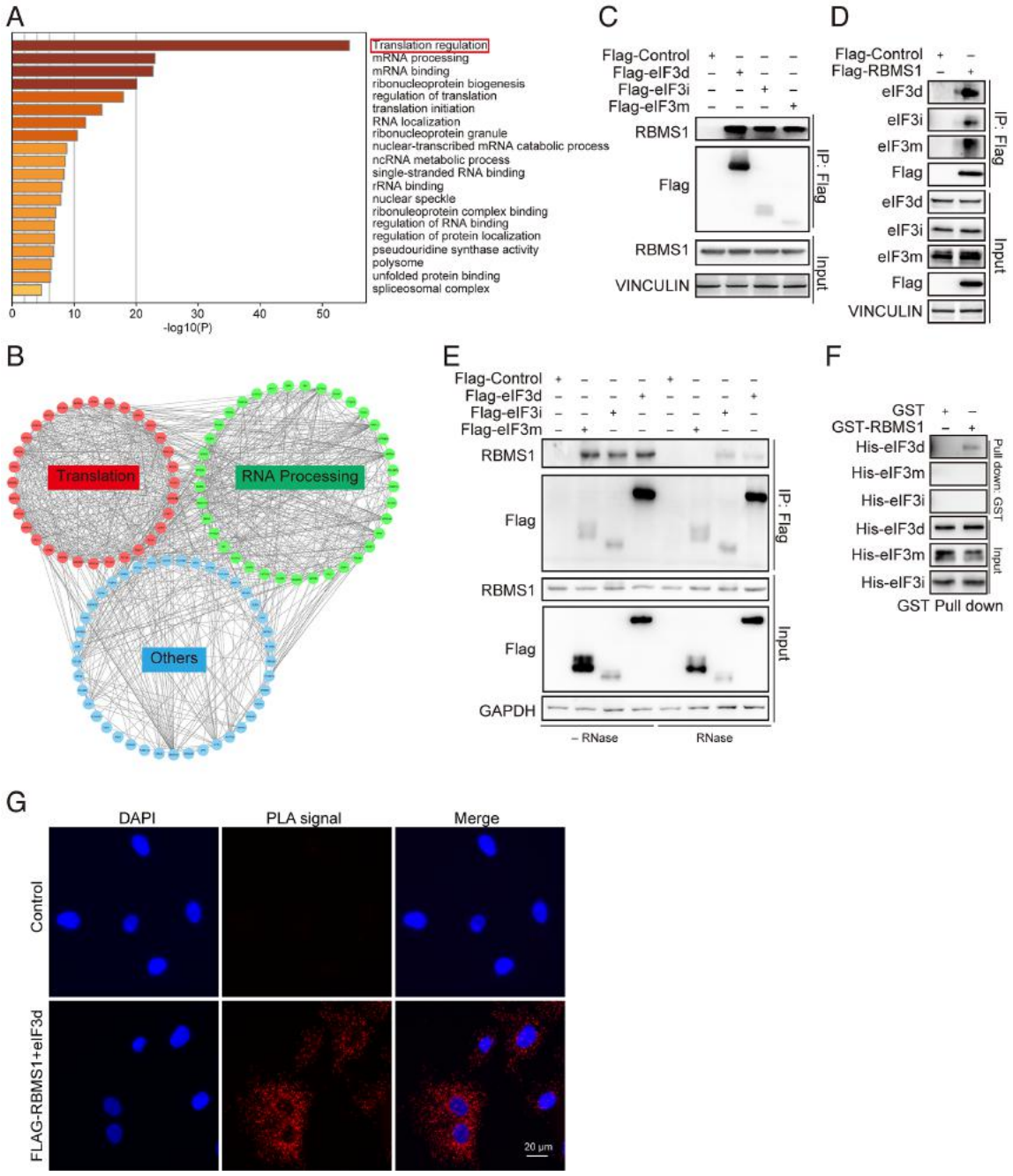

Figure 9. RBMS1 interacts with eIF3d. (A) Gene-ontology analysis of immunoprecipitation-coupled Mass-spectrometry using cells expressing RBMS1. **(B)** Functional-association network of genes from IP-MS were analyzed with STRING database. (**C-D**) Immunoprecipitation was performed in H1299 cells expressing Flag-eIF3d, Flag-eIF3i, or Flag-eIF3m respectively (C), or H1299 cells expressing Flag-

RBMS1 (D), and the precipitated-complexes were analyzed. **(E)** H1299 cells expressing Flag-eIF3d, Flag-eIF3i, or Flag-eIF3m respectively were applied to immunoprecipitation with/without RNase-A treatment, and the precipitated-complexes were analyzed. **(F)** GST-pull-down assays to analyze direct binding of recombinant human GST-tagged RBMS1 and His-tagged eIF3d, eIF3m, or eIF3i. (**G**) PLA was performed to examine the interaction between RBMS1 and eIF3d. PLA signals were shown in red and the nuclei in blue.

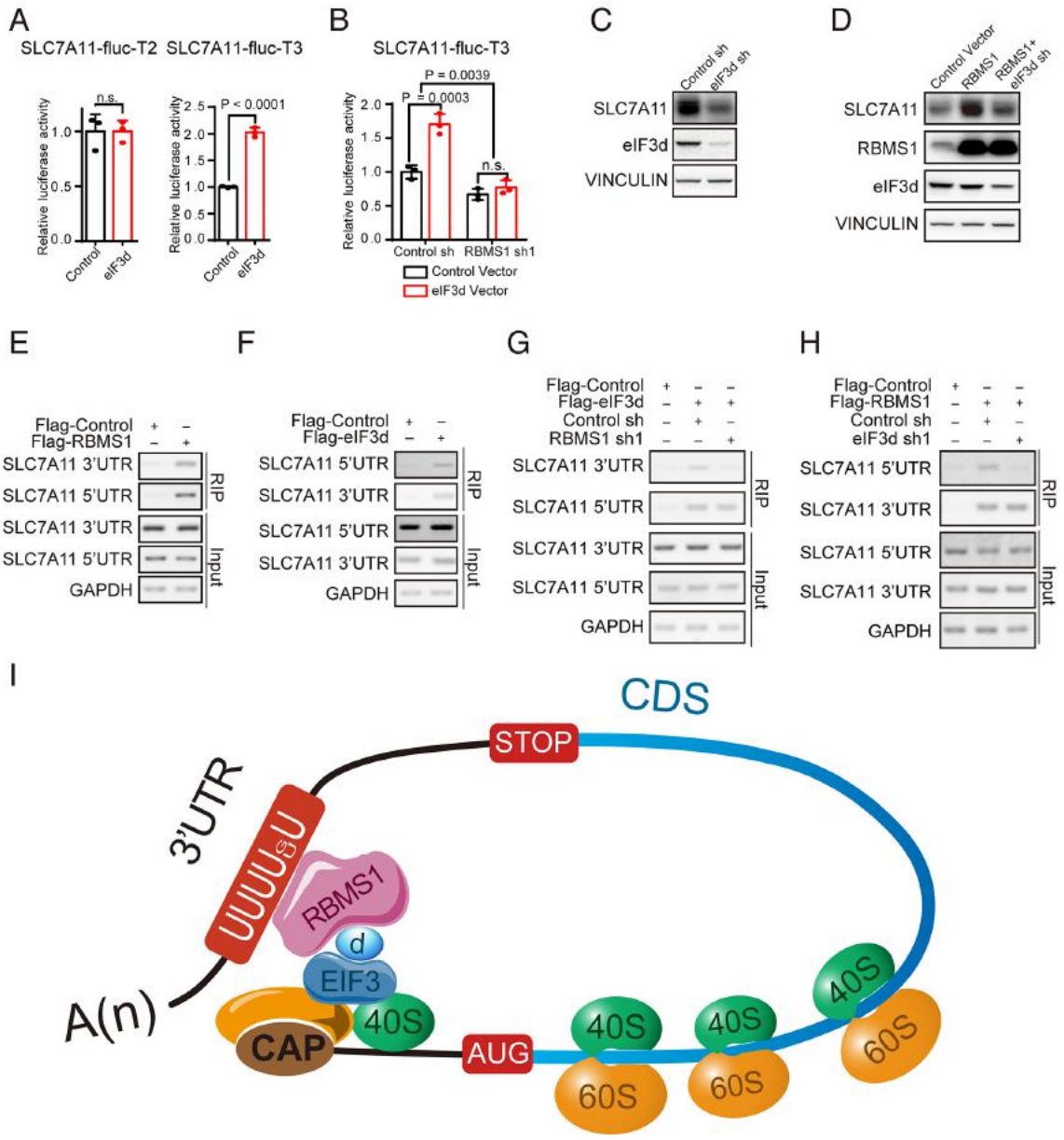

Figure 10. RBMS1 interacts with eIF3d to bridge the 3′- and 5′-UTR of SLC7A11 to promote its translation. (A) SLC7A11-fluc-T2 and SLC7A11-fluc-T3 were transiently transfected into eIF3d-expressed H1299 cells. **(B)** SLC7A11-fluc-T3 was transiently transfected into RBMS1-depleted H1299 cells with/without eIF3d expression. For (A-B), Data represent mean ± SEM (n = 3). P values were calculated from unpaired *t*-test in A; One-way ANOVA with Tukey's multiple comparisons in B. **(C)** The level of SLC7A11

was examined in H1299 cells with depleted-eIF3d. **(D)** The levels of SLC7A11, RBMS1, and eIF3d were examined in H1299 cells expressing RBMS1, with/without eIF3d-depletion. (**E**) Binding of *SLC7A11* 5′ and 3′-UTR with RBMS1 is examined by RNA-immunoprecipitation in A549 cells expressing FLAG-RBMS1. (**F**) Binding of *SLC7A11* 5′ and 3′-UTR with eIF3d is examined by RNA-immunoprecipitation in A549 cells expressing FLAG-eIF3d. (**G**) Binding of *SLC7A11* 3′- or 5′-UTR with eIF3d is examined by RNA-immunoprecipitation assay in A549 cells expressing FLAG-eIF3d with/without RBMS1 depletion. (**H**) Binding of *SLC7A11* 5′- or 3′-UTR with RBMS1 is examined by RNA-immunoprecipitation assay in A549 cells expressing FLAG-RBMS1 with/without eIF3d depletion. (**I**) Schematic of the model on how RBMS1 regulates the translation of SLC7A11.

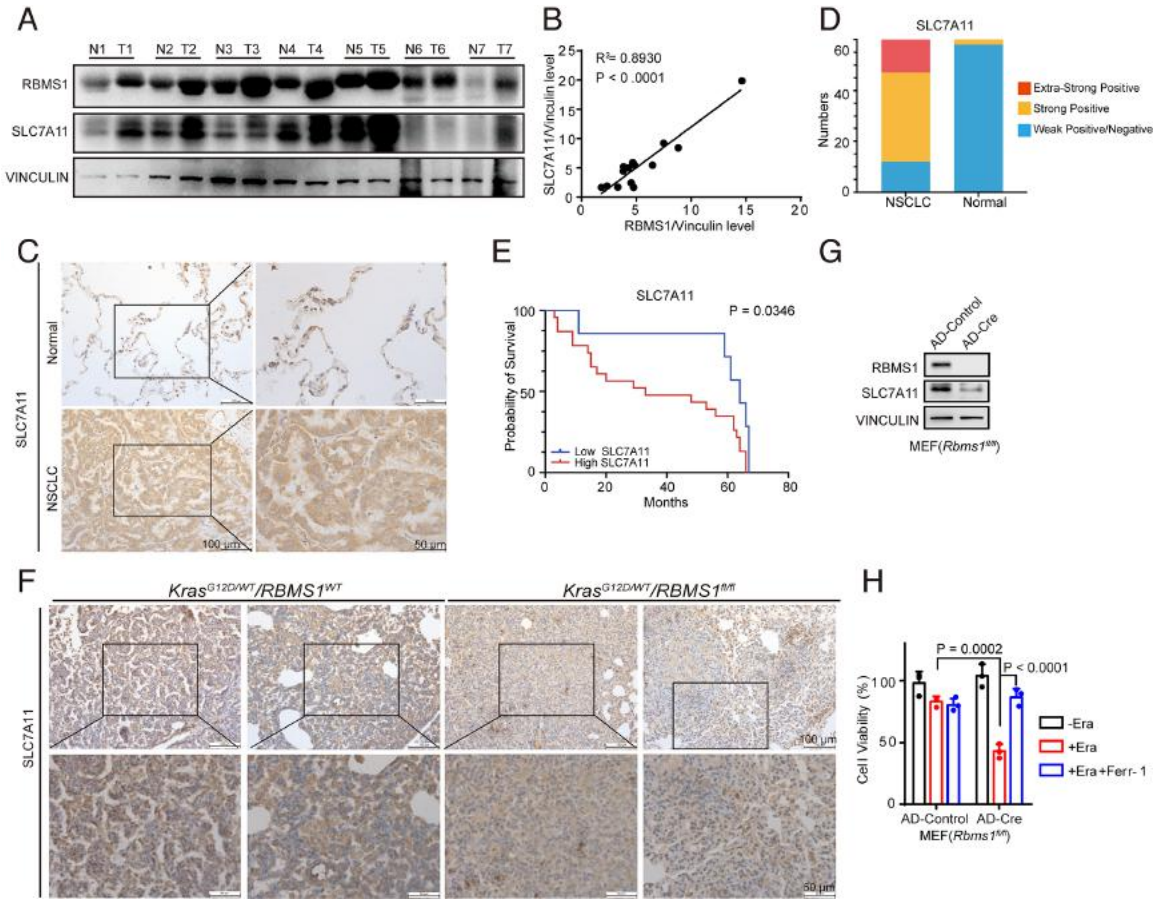

Figure 11 RBMS1 is positively correlated to SLC7A11 in clinical samples and mice. **(A)** RBMS1 and SLC7A11 levels of seven-pair lung-cancer patient tumors (T) and adjacent tissues (N) were analyzed. **(B)** Correlation of SLC7A11 and RBMS1 levels were analyzed. **(C)** Representative images from immunohistochemical-staining of SLC7A11 in lung cancers (n = 60) and normal tissues (n = 60). **(D)** The quantification of SLC7A11 level was classified into three-grades by immunohistochemical-staining. **(E)** Kaplan-Meier-curve showing overall-survival of lung cancers with high/low SLC7A11 expression. **(F)** Tumors were removed from *Kras*$^{G12D/WT}$/*Rbms1*^{WT} or CKO mice and subjected to immunohistochemical-staining with SLC7A11 antibody. **(G)** MEFs obtained from 14-day-old embryos of *Rbms1*$^{fl/fl}$ CKO mice were infected with Ad-Cre-virus to delete RBMS1. Levels of RBMS1 and SLC7A11 were examined. **(H)** Bar graphs

showing cell viability in RBMS1-deleted MEFs treated with erastin, with/without Ferr-1. Data represent as mean ± SEM (n = 3), P values were determined using One-way-ANOVA with Tukey's multiple comparisons in H.

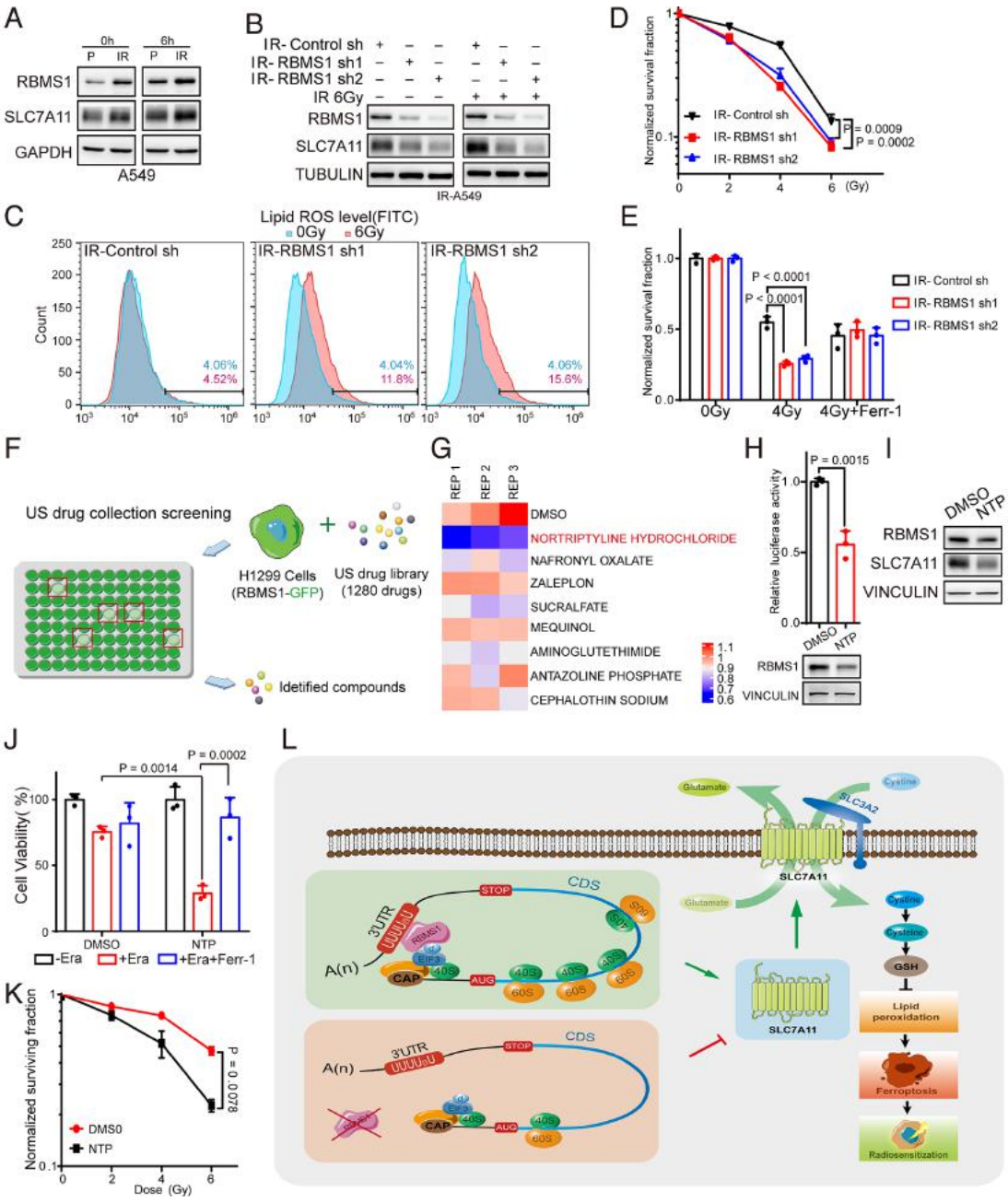

Figure 12 RBMS1 regulates lung cancer cell radioresistance through SLC7A11. (A-B) RBMS1 and SLC7A11 levels in irradiation-resistant A549 cells with/without irradiation (A), with/without RBMS1-depletion (B) were measured. **(C)** Lipid-peroxidation was measured by flow-cytometry after C11-BODIPY-staining in RBMS1-depleted IR-resistant A549 cells with/without irradiation. **(D-E)** Clonogenic survival was

examined in RBMS1-depleted IR-resistant A549 cells treated with different irradiation-dosages (D), or irradiation with/without Ferr-1 (E). **(F)** H1299 cells expressing pEGFP-RBMS1 were treated with 1280-compounds respectively. Fluorescence intensities were examined. **(G)** Heat-map depicting the GFP-intensity in A549 cells treated with eight identified-compounds respectively. **(H)** IR-resistant A549 cells were transfected with SLC7A11-fluc-T3, and treated with NTP. The luciferase-activities and RBMS1-level were examined. **(I)** RBMS1 and SLC7A11 levels in NTP-treated IR-resistant A549 cells were examined. **(J)** Bar graphs showing cell viability in IR-resistant A549 cells treated with NTP, erastin, with/without Ferr-1. **(K)** Clonogenic survival was examined in NTP-treated IR-resistant A549 cells with different irradiation-dosages. **(L)** The schematic of how RBMS1 regulates SLC7A11 translation and ferroptosis in lung cancer. Data represent as mean ± SEM (n = 3), P values were determined using One-way-ANOVA with Tukey's multiple comparisons in E, J; One-way repeated measures ANOVA in D, K; unpaired-t-test in H.